THE JOURNAL OF PHYSICAL CHEMISTRY C
A JOURNAL OF THE AMERICAN CHEMICAL SOCIETY

pubs.acs.org/JPCC Article

Elementary Steps in D_2−H_2O and H_2−D_2−H_2O Exchange Reactions on Pt Nanoparticles and Consequences of Liquid Water for the Binding and Reactivity of Chemisorbed Hydrogen

Samuel L. Leung, Sai Chen, and Enrique Iglesia*

Cite This: *J. Phys. Chem. C* 2023, 127, 22032−22048

Read Online

ACCESS | Metrics & More | Article Recommendations | SI Supporting Information

ABSTRACT: The identity and kinetic relevance of elementary steps and bound species in H_2O−D_2 and H_2−D_2−H_2O isotopic exchange on dispersed Pt nanoparticles are assessed as probes of the effects of chemisorbed and liquid water on surface-catalyzed exchange channels. The resulting rate equations consider the kinetically relevant chemisorption of H_2O and accurately describe the kinetic effects of H_2, D_2, and H_2O pressures on exchange rates. H_2−D_2 exchange is mediated by the reactions of H_2 and D* (or D_2 and H*) at “spaces” made available by local displacements of mobile H* or D* adatoms to alternate (atop to fcc) binding sites. Rate and equilibrium constants are similar for reactions under anhydrous conditions and in the presence of chemisorbed water. The additional exchange channels responsible for H_2O−D_2 exchange involve reactions between D_2 and molecularly adsorbed H_2O* also via “displacements” of hydrogen adatoms, as in the case of H_2−D_2 exchange. The formation of an intrapore liquid water phase via capillary condensation within the voids of γ-Al_2O_3, which contain the Pt nanoparticles, did not cause detectable changes in kinetic trends or in any of the parameters required to describe exchange rates. These undetectable effects of a dense liquid phase in contact with Pt nanoparticles are consistent with the absence of preferential solvation of transition states (TS) by liquids, which leads to nearly identical activity coefficients in the gas or liquid phase and considerations using TS formalisms of thermodynamically nonideal systems. The accurate interpretation of measured exchange rates required the removal of CO_2 contaminants from liquid water using procedures more stringent than those typically prescribed or used when water is present at the temperatures characteristic of isotopic exchange on metals.

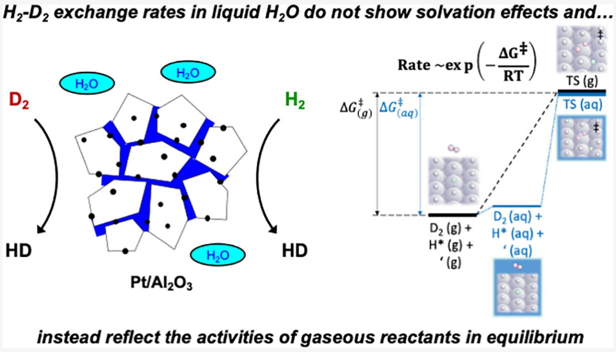

1. INTRODUCTION

Surface catalysis involves the binding of reactants, their chemical transformations, and the ultimate desorption of the products formed.[1] Understanding the nature of bound species and binding sites and the consequences of outer-sphere environments, such as a contacting liquid phase, is essential to interpret and design specific reaction channels for bound molecules. Dihydrogen dissociation and the reactions of bound H atoms (H*) mediate many useful reactions,[2−4] such as hydrogenolysis of alkanes[5−7] and hydrogenation of alkenes,[8−10] arenes,[11−13] and CO.[14−17] These processes have been probed using chemisorption,[18,19] calorimetry,[20−22] spectroscopy,[14,23,24] electrochemistry,[25−28] low-energy electron diffraction,[29,30] density functional theory (DFT),[31−33] and isotopic exchange methods.[34−37] These inquiries have addressed H-binding thermodynamics and H_2 dissociation dynamics in the absence of coadsorbed species[18,20,21,29,30,38−40] and also in the presence of alkanes,[5,41] CO,[42,43] and water.[14,27,34]

Isotopic exchange, as a method of inquiry, is useful to identify and probe the reversibility and kinetic relevance of elementary steps and to do so without disrupting the chemical steady state, thus providing uncorrupted, albeit indirect, details about the nature and prevalence of bound species and binding sites. The accurate interpretation of these data requires mechanistic insights into the elementary steps and their thermodynamics. The mechanism of H_2O−D_2 (or D_2O−H_2) isotopic exchange on Pt surfaces has been addressed in previous studies[14,27,34,44,45] but without rigorous mechanistic interpretations of exchange rates or any simultaneous assessments of the binding thermodynamics of bound species derived from H_2, D_2, and H_2O. In addition, the presence of trace contaminants in H_2O (as chemical impurities or dissolved gases) emerged in the present study as a potential ubiquitous corruption of previously reported exchange rates.

Received: July 11, 2023
Revised: September 29, 2023
Accepted: October 3, 2023
Published: November 1, 2023

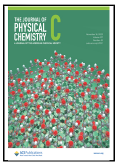

ACS Publications

https://doi.org/10.1021/acs.jpcc.3c04678

The present study addresses these mechanistic and experimental matters. It presents a unifying set of elementary steps that is consistent with all available kinetic and thermodynamic data, including insights and data from a previous study of H_2−D_2 exchange under anhydrous conditions.[37] The kinetic descriptions derived from these anhydrous data also accurately describe exchange rates in the presence of liquid H_2O, without requiring any modifications of the form of the expression or any evidence for effects of water, whether in gaseous, adsorbed, or liquid forms, on the kinetic or thermodynamic parameters involved in the reactions of chemisorbed H atoms (H* and D*). Such results reflect the minor consequences of liquid water as a solvent for the binding of H*/D* species and the transition states (TS) that mediate H_2−D_2 exchange.

Dissolved gases in liquid water can lead to unintended titration of metal surfaces. Their incomplete removal from reagents irreversibly affects exchange rates; these effects persist even after removing H_2O from the reactant stream. CO_2 is particularly challenging to remove through routine degassing protocols involving evacuation or extended flow of inert gases because it is present as solvated carbonate and bicarbonate ions.[46,47] When released into an inlet stream during the vaporization of liquid H_2O, gaseous CO_2 dissociates on metal surfaces at near ambient temperatures to form strongly bound CO (CO*) and O*;[48,49] the latter can be removed during contact with H_2 at near ambient temperature, but CO* (and its C* and O* dissociation products) requires significantly higher temperatures, thus leading to the irreversible titration of Pt surfaces during H_2−D_2 exchange on samples in contact with (or previously exposed to) contaminated H_2O.[50] The H_2O−D_2 and H_2O−H_2−D_2 kinetic studies presented here resort to atypically stringent precautions and procedures to remove dissolved CO_2.

The kinetics of H_2O−D_2 isotopic exchange are examined here on dispersed Pt nanoparticles in the presence of water but under conditions that either preclude or cause the formation of an intrapore liquid H_2O phase. The observed kinetic trends cannot be described using pathways proposed in earlier studies,[14,27,34,44,45] in the context of the surfaces saturated with H* and D* that prevail during exchange.[18,37] These trends indicate instead that HDO/D_2O and HD/H_2 form via reactions of D_2 with H_2O*, in steps that displace mobile D* (or H*) adsorbates to alternate binding locations (from atop to fcc), thus allowing D_2 to dissociate on "spaces" made accessible by such local displacements and then to exchange with H_2O*. These steps and the requisite competitive binding of D* and H_2O* are consistent with thermodynamic considerations from previous H_2 chemisorption studies,[18] as well as with theoretical and experimental evidence for the elementary steps that mediate H_2−D_2 exchange.[37] The proposed exchange pathways accurately describe exchange rates for D_2−H_2O and H_2−D_2−H_2O mixtures throughout a broad range of pressures (5−20 kPa of H_2, 10−40 kPa of D_2, and 0−20 kPa of H_2O); these pathways provide a framework to study the nature of hydrogen binding and reactions in the presence of water, whether in gaseous, physisorbed, or liquid forms.

Liquids impose an outer-sphere environment that can influence the binding of molecules as well as their reactivity, the latter through the preferential solvation of TSs and their relevant precursors. These outer-sphere effects have been implicated in modifications of the electronic properties of surfaces[34,51−53] and the binding of molecules involved in surface catalysis.[34,54] H_2O−H_2−D_2 reactions are used here to assess these effects through the formation of an intrapore liquid H_2O phase within γ-Al_2O_3 voids that contain Pt nanoparticles. These capillary condensation strategies allow a continuous transition from gas-filled to liquid-filled pore environments; they have been previously developed to examine the effects of nonpolar liquids on the reactions of hydrocarbons and oxygenates.[55,56] The measured H_2−D_2 exchange rates decreased monotonically as H_2O pressures increased, but these kinetic trends were not detectably distorted by the gradual formation of an intrapore liquid phase.

The observed effects of H_2O on H_2−D_2 exchange rates merely reflect the competitive adsorption of H_2O* and D* on Pt surfaces without any detectable consequences of a liquid phase for the stability of the bound exchange TSs or any perceptible electronic modification of Pt surfaces upon contact with liquid water. Pt surfaces mediate H_2−D_2 and H_2O−D_2 exchange by catalytic D_2 dissociation at spaces made available by local disruptions of dense mobile adlayers; exchange rates depend solely on H_2O pressure, irrespective of the physical state of water in the outer-sphere environment that contacts Pt nanoparticles. In all cases, competitive binding is driven by the contacting pressure of H_2O, irrespective of the presence or absence of H_2O in the liquid state.

2. METHODS

2.1. Catalyst Synthesis Methods. The γ-Al_2O_3 support (Sasol, CATALOX SBa 200) used to disperse Pt nanoparticles was treated in flowing dry air (0.83 $cm^3\ g^{-1}\ s^{-1}$; zero-grade; Praxair) by heating from ambient temperature to 1073 K at 0.083 K s^{-1} and holding for 5 h and then cooling to ambient temperature. Pt/γ-Al_2O_3 (1% wt. Pt) was prepared by incipient wetness impregnation of this γ-Al_2O_3 with a H_2PtCl_6 solution (8% wt. in H_2O, 0.26 $cm^3\ g^{-1}$ γ-Al_2O_3) and treated overnight in ambient air at 368 K. The sample was then exposed to flowing dry air (1.67 $cm^3\ g^{-1}\ s^{-1}$; zero-grade; Praxair), heated from ambient temperature to 873 K (0.083 K s^{-1}), and then held for 3 h. After cooling to ambient temperature, the sample was exposed to flowing H_2 (1.67 $cm^3\ g^{-1}\ s^{-1}$; 99.999% UHP; Praxair), heated to 1073 K (0.083 K s^{-1}), held for 2 h, and treated at ambient temperature in flowing 2% v/v O_2 (0.83 $cm^3\ g^{-1}\ s^{-1}$; balance He; certified grade, Praxair) for 0.5 h to passivate Pt nanoparticles before exposure to ambient air. Catalysts were heated in flowing H_2 (Praxair, UHP, 99.999% purity; 100 $cm^3\ g^{-1}\ s^{-1}$) to 873 K at 0.083 K s^{-1}, held for 2 h, and cooled to the target temperature before exchange experiments. Unsupported Pt powders (nominally 22.7 $m^2\ g^{-1}$ as provided, Strem Chemicals) were treated in flowing H_2 (400 $cm^3\ g^{-1}\ s^{-1}$, 99.999% UHP; Praxair) at 1073 K (0.083 K s^{-1}) for 2 h immediately before exchange rate measurements.

2.2. Pt Dispersion Measurements from H_2 Chemisorption Uptake. Pt dispersion (defined as the fraction of the total number of Pt atoms residing at nanoparticle surfaces) in Pt/γ-Al_2O_3 was measured from the H_2 uptake after heating the sample (~1 g) to 673 K (0.083 K s^{-1}) and holding for 1 h in flowing H_2 (0.33 $cm^3\ g^{-1}\ s^{-1}$; Praxair, UHP, 99.999% purity) and then exposing it to dynamic vacuum (to $<10^{-5}$ Pa) at 673 K for 1 h before cooling to 373 K. Uptake values were measured by the sequential dosing of known amounts of H_2 into a known sample volume containing the sample at different H_2 pressures (1−40 kPa H_2). Saturation uptake values were obtained from the uptake values extrapolated to zero pressure

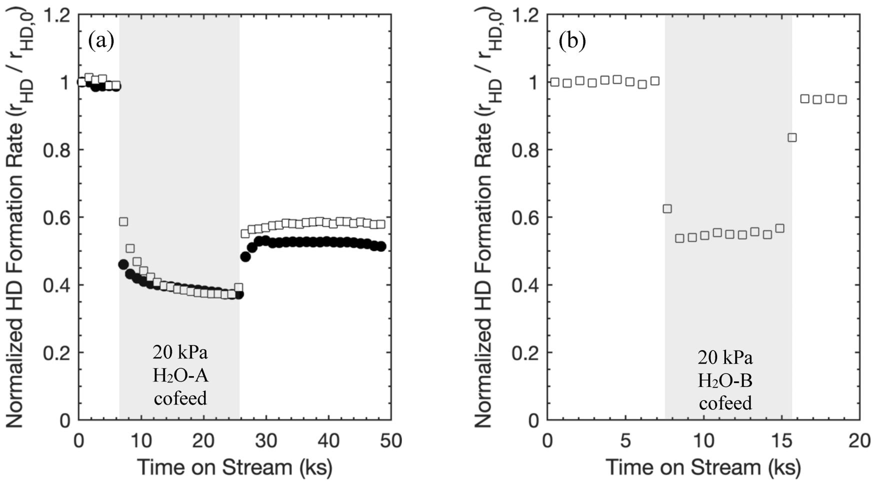

Figure 1. HD formation rates (20 kPa H_2 and 20 kPa D_2), normalized by initial rates ($r_{HD,0}$), on (●) Pt powders and (□) Pt/γ-Al_2O_3 at 473 K before, during (shaded region), and after exposure to 20 kPa (a) H_2O-A and (b) H_2O-B, treated as described in Section 2.3.

to remove the contributions from weakly bound H* species. The dispersion of Pt in the Pt/γ-Al_2O_3 samples measured by these methods was 0.72. This dispersion corresponds with an average crystallite diameter of 1.9 nm, calculated using established methods that account for the suprastoichiometric H/Pt_s ratios at edge and corner sites (details in Section SI-1.1).

2.3. H_2−D_2, H_2O−D_2, and H_2O−H_2−D_2 Isotopic Exchange Rates. Isotopic exchange turnover rates (units: s^{-1}; normalized by the number of Pt surface sites) were measured on aggregates (<100 μm) of unsupported Pt powders (0.1−0.5 mg) and Pt/γ-Al_2O_3 (0.5−5 mg) held on a quartz frit within a U-shaped quartz tube (6.35 mm O.D. and 4 mm I.D.). H_2 (99.999% UHP; Praxair), D_2 (99.8% isotopic enrichment, research-grade; Praxair), and N_2 (99.998%, Praxair) were purified using O_2 and H_2O traps (VICI Metronics). Inlet molar rates were metered with electronic mass flow controllers (Parker-Porter 200 series).

Deionized H_2O (>18.0 MΩ cm) was further treated by bubbling inert N_2 at ambient temperature for more than 24 h. This water (denoted as H_2O-A) contains trace dissolved gases and was therefore treated further by exposing to dynamic vacuum at 363 K for 6 h, until about 80% of the starting liquid volume had evaporated (denoted as H_2O-B). Such extreme degassing procedures were essential to fully remove dissolved gases, specifically CO_2, which dissociates to form strongly bound CO at the conditions of the exchange experiments (such strong effects of traces of CO_2 are shown in Sections 3.1 and SI-3). H_2O (H_2O-A or H_2O-B) was injected into the flowing gases at 423 K by using a syringe pump (KD Scientific Legato 200).

The concentrations of all reactants and deuterated species (H_2, HD, D_2, H_2O, HDO, D_2O, and N_2) in the effluent were determined using mass spectrometry (Leybold Inficon Transpector, TSP TH200). H_2−D_2 exchange rates were calculated from these data and corrected for their approach to the binomial distribution expected at equilibrium[57] at these reaction temperatures (>473 K) to determine the forward rates without contributions from reverse reactions, thus simplifying the mechanism-based equations derived for exchange rates (details in Section SI-1.2).

Reaction rates on Pt powders were normalized using H_2−D_2 exchange to measure the number of active sites at 373 K (20 kPa H_2 and 20 kPa D_2). Turnover rates were assumed to be similar to those on Pt/γ-Al_2O_3, based on H_2−D_2 exchange rates shown to be insensitive to nanoparticle diameters (1.5−3.2 nm) in previous studies.[37] This approach is necessary because Pt powders sinter significantly[58−60] during H_2 treatment at 1073 K (Section 2.1); such high-temperature treatments were necessary to ensure that additional structural changes did not occur during the reaction, thus corrupting kinetic studies. The small amount of Pt powders (ca. 0.5 mg) used in these experiments and the low surface area following sintering, required to be able to achieve differential conversions, were not amenable to surface area measurements or to particle size estimates from chemisorption uptake. Larger quantities of Pt powders may sinter to different extents and are therefore not reflective of the effective Pt dispersion detected by H_2−D_2 exchange. Assuming that H_2−D_2 isotopic exchange rates can be used as an accurate measure of the active surface area, these Pt powders exhibited a particle diameter of approximately 400 nm (calculated using the methods described in SI-1.1). The absence of transport effects were ruled out by nearly identical activation energies for H_2−D_2 isotopic exchange on Pt powders and Pt/γ-Al_2O_3 (27.2 ± 0.3 vs 30.1 ± 0.2 kJ mol^{-1}, respectively) that did not curve in an Arrhenius plot with changes in temperature when varying the catalyst aggregate size, as in our prior study.[37]

2.4. Textural Properties of γ-Al_2O_3 and Calculation of H_2O Adsorption Isotherms. N_2 uptakes on γ-Al_2O_3 were measured at the normal boiling point of N_2 (77 K; Micromeritics 3Flex Adsorption Analyzer) (Section SI-2). The γ-Al_2O_3 sample (ca. 100 mg) was treated by heating from ambient temperature to 673 at 0.17 K s^{-1} and holding for 3 h under vacuum before these measurements. The pore size distribution was obtained from these uptake data using the Barret−Joyner−Halenda (BJH) equation,[61] which considers vapor pressure, molar volume, and surface tension of a liquid for any given molecule. The pore size distribution was obtained from the N_2 uptake at the normal boiling point and then used to estimate the H_2O uptake (and the extent of intrapore capillary condensation) at 323 K using the BJH equation and the molar properties of H_2O at 323 K, as reported previously for nonpolar liquids in mesoporous silica[55] and TiO_2.[56] This method provides an estimate of the fraction of the γ-Al_2O_3 void volume that is filled with liquid H_2O at

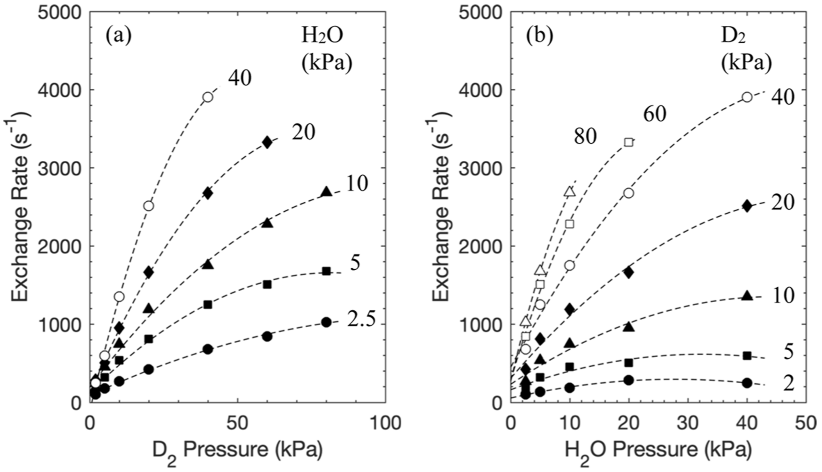

Figure 2. H_2O-D_2 isotopic exchange rates on Pt/γ-Al_2O_3 at 473 K at different (a) D_2 pressures (2.5 (●), 5 (■), 10 (▲), 20 (◆), and 40 (○) kPa H_2O) and (b) H_2O (H_2O-B) pressures (2 (●), 5 (■), 10 (▲), and 20 (◆), 40 (○), 60 (□), and 80 (Δ) kPa D_2). Dashed lines are added to guide the eye.

each condition during isotopic exchange experiments with D_2-H_2O and $H_2-D_2-H_2O$ reactant mixtures.

3. RESULTS AND DISCUSSION

3.1. Effects of Dissolved CO_2 in H_2O on H_2-D_2 Isotopic Exchange Rates. Ultrapure water, free of any traces of CO_2, is essential to obtain uncorrupted isotopic exchange rate data and to prevent inaccurate mechanistic assignments because CO_2 acts as a precursor to stoichiometric titrants (CO and its dissociation products) of nanoparticle surfaces at low temperatures. These artifacts are demonstrated here by comparing the results with H_2O treated using customary degassing protocols (Section 2.3; 18.0 MΩ cm; H_2O-A) and with more stringent procedures (Section 2.3; H_2O-B); these artifacts are avoided here using H_2O subjected to more stringent degassing procedures, which are then used in all other experiments (H_2O-B; Section 2.3) reported in this study. HD formation rates were measured on Pt/γ-Al_2O_3 and on unsupported Pt powders before, during, and after exposure to H_2O-A or H_2O-B.

Figure 1 shows HD formation rates (normalized to the rates measured upon initial contact with reactants, $r_{HD,0}$) as a function of the time elapsed in contact with reactants by using (a) H_2O-A or (b) H_2O-B in the reactant mixtures. H_2-D_2 exchange rates were stable under anhydrous conditions (Figure 1a, $t < 6$ ks) but decreased upon contact with 20 kPa H_2O-A on both Pt/γ-Al_2O_3 and Pt powders (Figure 1a, 6−26 ks, as indicated by the shaded region) and ultimately reached constant values. Rates increased instantaneously when H_2O-A was removed from the inlet stream (26 ks, Figure 1a), but the rates were not restored to the initial values even after 20 ks (0.58 ± 0.03 and 0.52 ± 0.02 fractions of the initial rates on Pt/γ-Al_2O_3 and Pt powders, respectively); these irreversible titration effects are unrelated to the support effects, as demonstrated by the similar effects observed on both samples. They seem to reflect either the restructuring or titration of Pt nanoparticles, which cannot be reversed upon the removal of water at 473 K; any consequences of using water coreactants with different trace impurities would confirm the latter interpretation.

Figure 1b shows that HD formation rates decreased upon contact with H_2O-B (indicated by the shaded region), which, in contrast with the data in Figure 1a, are recovered to initial rates after removal of H_2O from the inlet stream. The concentration of any trace impurities removed by more extensive degassing (to prepare H_2O-B) cannot plausibly influence the extent of any restructuring. These data implicate impurities that can be removed from liquid H_2O by more stringent degassing as the origins of the lower rates and the incomplete restoring of initial rates when H_2O-A is used.

CO_2 dissolves in H_2O at appreciable concentrations upon contact with ambient air;[47] it dissociates on Pt metal surfaces at near ambient temperatures to CO* and O* and also reacts with O* to form stable bidentate carbonates.[50] O* is readily removed by H_2 at the typical temperatures of H_2-D_2 exchange (383−473 K), but CO* and carbonates desorb (and/or react with H_2) only at higher temperatures. Pt powders exposed to H_2O-A during exchange measurements (10 kPa H_2, 10 kPa D_2, 20 kPa H_2O, 20 ks, 473 K) were used for anhydrous exchange reactions with H_2-D_2 mixtures 10 kPa H_2 and 10 kPa D_2) as the reaction temperature was gradually increased to 823 K (at 0.033 K s^{-1}); exchange rates were fully restored when measured again at 473 K after such temperature cycling (Figure SI-2, Section SI-3.1). A similar temperature cycle with N_2 did not restore initial rates, apparently because of the dissociation of some CO* species or the formation of carbonate species before desorption or reaction (Figure SI-2, Section SI-3.1). Contact with CO_2 (0.4 kPa for 3.6 ks) similarly led to lower H_2-D_2 exchange rates (0.36 ± 0.02 times the initial rate) during its cofeed (Figure SI-3, Section 3.1); these rates recovered slightly after CO_2 was removed but reached asymptotic rates lower than those before exposure to CO_2 (0.44 ± 0.05 times the initial rate) after 3 ks, similar to the effects observed in the data shown in Figure 1a using H_2O-A. These data implicate dissolved CO_2 (through its surface reactions to form CO) as the trace contaminant in H_2O-A; the presence of such contaminants causes significant kinetic artifacts that, if unrecognized or eliminated, could be inaccurately interpreted as an effect of water on the binding of hydrogen adatoms; such artifacts remain consequential whether H_2O is present in its gaseous, bound, or liquid states. They can be avoided using the degassing procedure described in Section 2.3 and H_2O-B has been used in all experiments described below. These treatments may seem obvious in

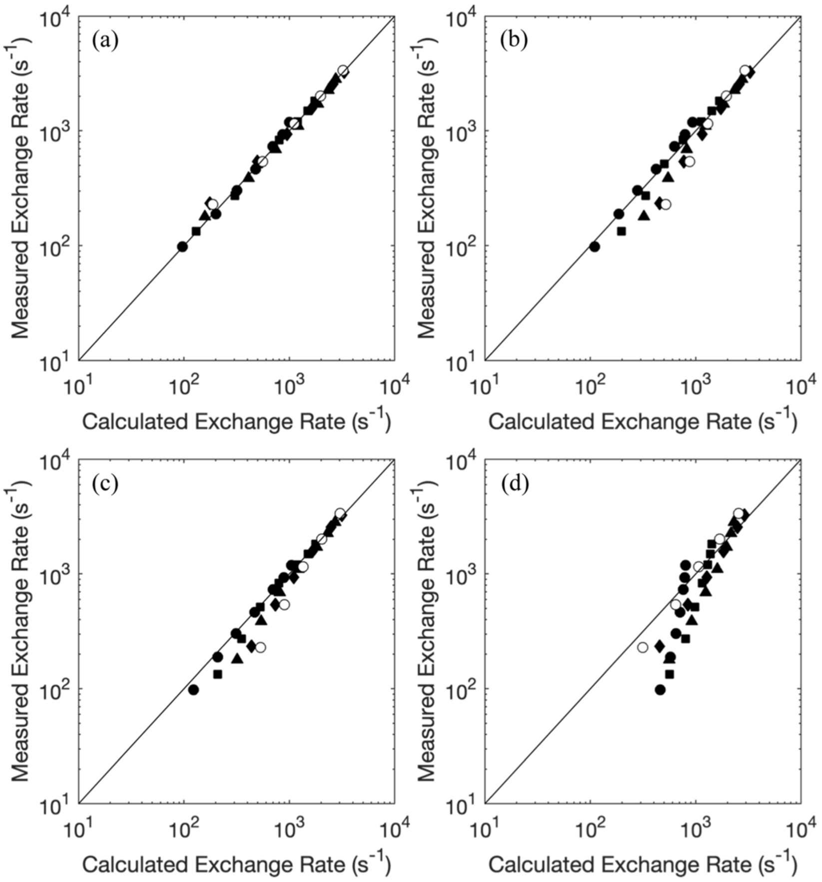

Figure 3. Measured and calculated (from regressed rate parameters) H_2O−D_2 isotopic exchange rates on Pt/γ-Al_2O_3 at 473 K mediated by the reactions of (a) H_2O(g) and D*, (b) H_2O* and D*, (c) H_2O* with D′ (H_2O* and D′ are adsorbed at distinct noncompeting sites), and (d) H_2O dissociation (to form OH* and H*) and recombination of OH* and D* at (●) 2.5, (■) 5, (▲) 10, (◆) 20, and (○) 40 kPa H_2O-B. Calculated rates were obtained by regressing the data to the function form of the rate equations associated with each pathway (details in Section 3).

retrospect, but we consider it essential to inform about these matters because they are required for obtaining uncorrupted data and for ensuring their unequivocal mechanistic interpretations and were not recognized during the initial stages of our study.

3.2. Kinetic Trends and Analysis of Isotopic Exchange Rates on H_2O and D_2 Pressures. Forward turnover rates of H_2O−D_2 exchange are defined here as the (equal) rates of disappearance of D_2 and H_2O (which are also equal to the combined rates of HD and H_2 or HDO and D_2O formation, respectively). They were measured on Pt/γ-Al_2O_3 at 2−40 kPa H_2O-B (treated as described in Section 2.3), 2−80 kPa D_2, and 473 K. Exchange rates increased with increasing H_2O and D_2 pressures (sublinearly, Figure 2).

Several reaction channels were examined in order to assess their ability to account for these kinetic trends; these included some previously proposed routes involving reactions of (a) H_2O(g) with D*,[34] (b) H_2O* with D*,[44] and (c) H_2O* with D′[45] (with the previously invoked ad hoc assumption that H_2O* and D′ bind at distinct noncompeting sites) as kinetically relevant steps. H_2O dissociation (to form OH* and H*) and the recombination of OH* and D* (d) were also considered because such steps have been proposed to occur on Pt surfaces during water−gas shift reactions.[62−64] The reaction schemes (Schemes SI-2−SI-5) for pathways (a−d) and their respective rate equations (eqs SI-20, SI-37, SI-56, and SI-83) and derivations are included in the Supporting Information (Section SI-4). The rate constants and equilibrium constants in these equations were obtained by regressing all of the data in Figure 2 to the respective functional forms of the rate equations by minimizing the sum of the squares of relative deviations between measurements and model predictions; the results of these regressions are shown as parity plots in Figure 3.

Figure 3 demonstrates that pathways (b−d) cannot accurately describe the measured rates. Moreover, the regressed value of the equilibrium constant (K_3) for D_2 dissociative adsorption

$$D_2 + 2^* \overset{K_3}{\rightleftarrows} 2D^* \tag{1}$$

in each of these pathways was very small (Tables SI-2−SI-4 and Section SI-4; $<1.5 \times 10^{-12}$ kPa^{-1}) and would lead to Pt nanoparticle surfaces that remain essentially bare at the conditions of these measurements (fractional coverages $<10^{-5}$; 5−80 kPa D_2). Such low coverages stand in contrast with the saturated D* coverages observed under anhydrous conditions on 1.6 nm Pt particles under these conditions (2−80 kPa D_2 and 473 K) and even at higher temperatures.[18,37] Pathway (a) was able to describe rate data modestly well; the large uncertainty in the regressed equilibrium constant for D_2 dissociative adsorption ($K_3 = 2.4 \times 10^{-14} \pm 24$ kPa^{-1}; eq 1) indicates that the model is relatively insensitive to the surface coverages of D adatoms. Thus, in order to visualize deviations in the experimental data from the model at expected D* coverages, the data (Figure 2) were also regressed to the relevant rate equation for pathway (a) (eq SI-20 and Section SI-4) by setting the value of K_3 to that estimated (1.4 kPa^{-1}; 473 K) from the average enthalpy and entropy of adsorption (−43 kJ mol^{-1} and −50 J mol^{-1} K^{-1}) measured previously from H_2 dissociative chemisorption studies[18] ($\Delta H_{H2}{}^{\circ} = -40$ to −46 kJ mol^{-1}, 0.5 ML; $\Delta S_{H2}{}^{\circ} = -20$ to −80 J mol^{-1} K^{-1}, 0.2−1.0 ML), which shows thermodynamic isotope effects near unity.[37] The resulting model descriptions show systematic deviations from the measured rates, as shown in Figure 4.

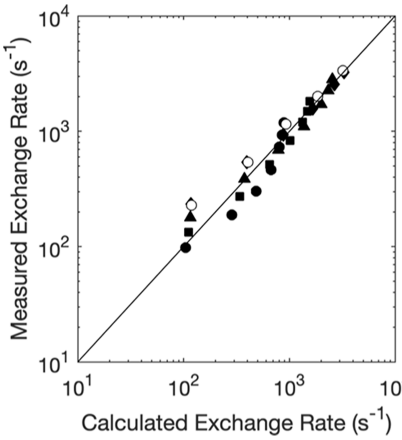

Figure 4. Measured and calculated (from regressed rate parameters) H_2O-D_2 isotopic exchange rates on Pt/γ-Al_2O_3 at 473 K mediated by reactions of $H_2O(g)$ and D* (pathway (a)) at (●) 2.5, (■) 5, (▲) 10, (◆) 20, and (○) 40 kPa H_2O-B. Calculated rates were obtained using a fixed value for K_3 (1.4 kPa^{-1}), estimated from prior chemisorption studies.[18]

Pathways b−d were also examined using similar protocols (described in Section SI-4) and showed significantly larger deviations than those in Figure 3, as expected. These pathways (a−d) were therefore discarded and considered to be inconsistent with the combined chemisorption and exchange rate data.

3.3. H_2O-D_2 Isotopic Exchange Pathways on Pt/γ-Al_2O_3.

H_2-D_2 exchange on surfaces saturated with H* and D* occurs via the dissociative adsorption of H_2 (or D_2) at spaces arising from the displacement of adatoms to alternate binding modes (e.g., atop vs fcc).[37] H_2O may also adsorb on Pt surfaces, competing with hydrogen adatoms. Thus, another plausible H_2O-D_2 exchange pathway involves D_2 dissociation to D* (step 1.1, Scheme 1) and competitive adsorption with the H_2O* species formed in step 1.2 (Scheme 1). H_2O* can then desorb (step 1.3, Scheme 1) or exchange its H-atoms with D_2 molecules that bind via noncompetitive displacements of D*, leading to the formation of HDO* and HD (step 1.5, Scheme 1). The desorption of HDO* (step 1.4, Scheme 1) then completes an isotopic exchange event, while additional exchange between HDO* and D_2 would ultimately form D_2O* (step 1.6, Scheme 1). As in H_2-D_2 exchange, the seemingly "direct" (i.e., Eley−Rideal) reactions of $D_2(g)$ with H_2O* (steps 1.5 and 1.6, Scheme 1) are likely to involve a series of steps in which D_2 dissociates at vacancies that form via the local displacement of mobile D* species onto vicinal locations, where they assume alternate binding modes (atop vs fcc) within D*−H_2O* adlayers, followed by fast exchange between these D* adatoms and H_2O*; such routes can leave the kinetic impression of a direct reaction between a gaseous D_2 molecule and H_2O*.

The steps and reversibility assumptions in Scheme 1 are used next to derive an equation for H_2O-D_2 exchange rates (defined as the rate of disappearance of H_2O or D_2 isotopologs; $r_{D_2,f} = r_{H_2O,f}$) using pseudo-steady-state formalisms for all bound species. The derivation includes kinetic isotopic effects for H_2O desorption (steps 1.2−1.4, Scheme 1) and for D_2 reactions with H_2O* (H_2O* and HDO*) (steps 1.5−1.6, Scheme 1) near unity, an inference derived from independent H_2-D_2 isotopic exchange data (and by the similarity between the proposed TS for H_2O-D_2 exchange and H_2-D_2 exchange). Exchange rates derived using these protocols and assumptions are described by

$$\begin{aligned}-r_{D_2,f} &= -r_{H_2O,f}\\ &= r_{HDO,f} + r_{D_2O,f}\\ &= \frac{k_6(H_2O)(D_2)}{\left((H_2O) + \frac{\sqrt{K_3}}{K_5}\sqrt{(D_2)}\right)\left(1 + \frac{k_6}{k_{-5}}(D_2)\right)}\end{aligned} \qquad (2)$$

where k_i and K_i are the rate and equilibrium constants for step i in Scheme 1 (derivation details in SI-5.1). The three parameters (k_6, $\frac{\sqrt{K_3}}{K_5}$, and k_{-5}; eq 2) were estimated regressing all rate data (Figure 2) to the functional form of eq 2. Their values are 121 ± 8 kPa^{-1} s^{-1}, 2.1 ± 0.3 $kPa^{0.5}$, and (4.0 ± 2.4) × 10^4 s^{-1}, respectively. A sensitivity analysis to determine of how each parameter accounts for the regression uncertainties (shown in Section SI-6) shows that k_6, $\frac{\sqrt{K_3}}{K_5}$, and $\frac{k_6}{k_{-5}}$ can all be determined with certainty from these data. Figure 5 shows the excellent agreement for the measured H_2O-D_2 exchange rates (over a 100-fold range) and those predicted from eq 2 and the value of its regressed parameters. The $\frac{\sqrt{K_3}}{K_5}$ term represents the ratio of equilibrium constants for D_2 dissociative adsorption and H_2O molecular adsorption and leads to $\frac{\theta_D}{\theta_{H_2O}}$ estimates between 0.13 and 34 for the H_2O and D_2 pressure ranges (2−40 kPa H_2O and 2−80 kPa D_2) used here (Figure 2); these relative coverages are given by

$$\frac{\theta_D}{\theta_{H_2O}} = \frac{\sqrt{K_3}}{K_5}\frac{(D_2)}{(H_2O)} \qquad (3)$$

These values of $\frac{\theta_D}{\theta_{H_2O}}$ indicate that D* and H_2O* coverages are both kinetically consequential at the conditions used to measure the exchange rates shown in Figure 2 (2−40 kPa H_2O and 2−80 kPa D_2, 473 K). The presence of H_2O* at consequential coverages seems at odds with its propensity to desorb readily from Pt surfaces at low temperatures (∼200 K).[65,66] Yet, H_2O adsorption enthalpies on Pt(111) surfaces (−51.3 ± 1.6 kJ mol^{-1}, 0.5 ML H_2O)[67,68] are similar in magnitude to those for dissociative H_2 adsorption (−40 to −46 kJ mol^{-1}, 0.5 ML, 1.6 nm Pt particles).[18] The temperatures (>400 K)[69] required for the desorption of H* (or D*) from Pt surfaces may reflect higher energy barriers and smaller entropy loss (due to the mobility of H* adatoms) associated with the recombination of H*/D* adatoms compared to the molecular desorption of H_2O. Equation 2 and its mechanistic under-

Scheme 1. Elementary Steps for H_2O-D_2 and $H_2O-H_2-D_2$ Isotopic Exchange Reactions Mediated by $D_2-H_2O^*$ Reactions[a]

H_2O-D_2 Exchange Elementary Steps

$$D_2 + 2^* \xrightleftharpoons[k_{-3}]{k_3} 2D^* \quad [1.1]$$

$$H_2O + ^* \xrightleftharpoons[k_{-5}]{k_5} H_2O^* \quad [1.2]$$

$$HDO + ^* \xleftarrow[k_{-5}]{} HDO^* \quad [1.3]$$

$$D_2O + ^* \xleftarrow[k_{-5}]{} D_2O^* \quad [1.4]$$

$$D_2 + H_2O^* \xrightarrow{k_6} HD + HDO^* \quad [1.5]$$

$$D_2 + HDO^* \xrightarrow{k_6} HD + D_2O^* \quad [1.6]$$

Additional Steps for H_2O-H_2-D_2 Exchange

$$H_2 + 2^* \xrightleftharpoons[k_{-1}]{k_1} 2H^* \quad [1.7]$$

$$HD + 2^* \xleftarrow[k_{-2}]{} H^* + D^* \quad [1.8]$$

$$H_2 + D^* \xrightarrow{k_4} HD + H^* \quad [1.9]$$

$$D_2 + H^* \xrightarrow{k_4} HD + D^* \quad [1.10]$$

$$H_2 + HDO^* \xrightarrow{k_6} HD + H_2O^* \quad [1.11]$$

$$H_2 + D_2O^* \xrightarrow{k_6} HD + HDO^* \quad [1.12]$$

[a] Kinetic and thermodynamic isotopic effects are assumed to be near unity.

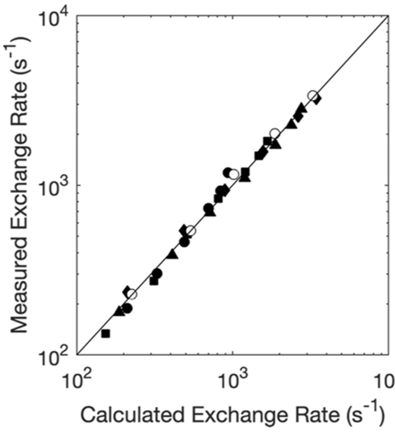

Figure 5. Measured exchange rates vs those obtained by regression of all rate data in Figure 2 to the functional form of eq 2 (corresponding to the elementary steps in Scheme 1) at (●) 2.5, (■) 5, (▲) 10, (◆) 20, and (○) 40 kPa H_2O.

pinnings accurately account for all measured kinetic trends in H_2O-D_2 exchange rates; they are also consistent with the saturation coverages of hydrogen adatoms reported in earlier studies at pressures and temperatures similar to those used to measure exchange rates.[18,37] This contrasts with the inaccurate descriptions of measured exchange rates based on alternate mechanisms proposed in previous studies (pathways (a–d); Section 3.2).

3.4. Consequences of Bound H_2O Molecules as Reactive Intermediates in H_2O-D_2 Exchange.

H_2O^* adsorbs competitively with D^* (and H^*) at kinetically detectable coverages ($\frac{\theta_D}{\theta_{H_2O}} = 0.13-34$, eq 3) and acts as a reactive intermediate that forms not only HDO^* (step 1.5, Scheme 1) but also D_2O^* (step 1.6, Scheme 1) as primary products (in a single surface sojourn) via sequential D_2 reactions, without requiring the intervening desorption and readsorption of HDO. These steps stand in contrast with alternate routes that do not involve bound H_2O molecules as direct reactive species (e.g., $H_2O(g) + D^*$, pathway (a) in Section 3.2);[34] these alternate routes can form D_2O only through subsequent readsorption of gaseous HDO but not in a single surface sojourn. D_2O formation rates (and the ratio of D_2O/HDO) extrapolated to zero residence time are thus expected to be nonzero if exchange occurred via the pathways described in Scheme 1.

Figure 6 shows D_2O/HDO ratios at different bed residence times (20 kPa H_2O, 20 kPa D_2, and 473 K) on Pt powders; the asymptotic ratio is 0.056 ± 0.002 (Figure 6). This ratio reflects the relative rates of D_2O^* and HDO^* desorption as primary products (steps 1.3 and 1.4, Scheme 1) and, in turn, their relative coverages on Pt surfaces (in the absence of significant kinetic and thermodynamic isotope effects). This nonzero value, indicative of the ability of D_2O to form in a single surface sojourn, provides compelling evidence for kinetically competent bound H_2O species as intermediates in D_2-H_2O

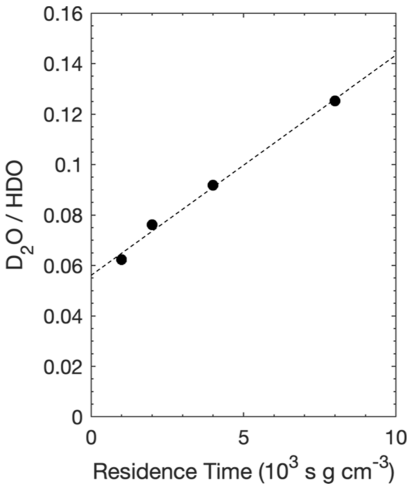

Figure 6. D_2O/HDO isotopic ratio as a function of bed residence time during H_2O-D_2 reactions on Pt powders (20 kPa H_2O and 20 kPa D_2, 473 K). Dashed line represents the regression of these data to a linear functional form.

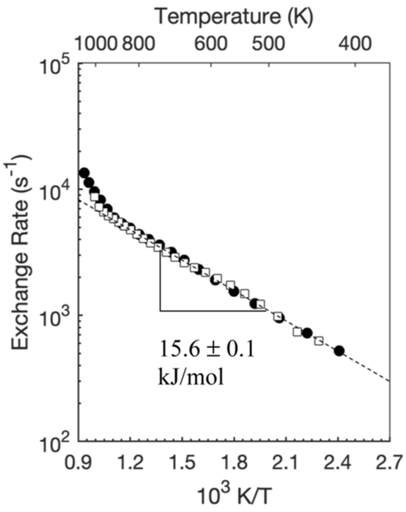

Figure 7. Arrhenius plot of H_2O-D_2 isotopic exchange rates on Pt/γ-Al_2O_3 (●) and Pt powders (☐) at 5 kPa of H_2O and 40 kPa of D_2 between 423 and 1073 K. Dashed line represents linear regression of data between 423 and 873 K.

exchange. The asymptotic ratio predicted by the reaction channel depicted in Scheme 1 is (derivation in Section SI-5.2)

$$\frac{r_{D_2O}}{r_{HDO}} = \frac{k_6(D_2)}{2k_{-5}} \tag{4}$$

The regressed values of k_6 (121 ± 9 kPa^{-1} s^{-1}) and k_{-5} ((4.0 ± 2.4) × 10^4 s^{-1}), obtained independently from the regression of exchange rate data in Figure 2 to the functional form of eq 2, and the D_2 pressure used in the residence time experiments (20 kPa) give an asymptotic D_2O/HDO ratio of 0.061 ± 0.037, in excellent agreement with the measured values (0.056 ± 0.002, Figure 6). These results are consistent with the mechanistic underpinnings provided by the steps in Scheme 1; they contradict the predictions from alternate pathways that do not involve bound H_2O^* at the surfaces as mediators of exchange turnovers (e.g., pathway (a); Section 3.2).

3.5. Effects of Pt Nanoparticle Size on H_2O-D_2 Exchange Activation Barriers.

H_2O-D_2 exchange rates (5 kPa H_2O-B, 40 kPa D_2) were measured at different temperatures (423−1073 K) on Pt/γ-Al_2O_3 and Pt powders in order to estimate the activation energies (Figure 7). Differences in activation energy are expected when the rate of a given reaction is sensitive to Pt surface coordination and thus nanoparticle size.[70−72] The apparent activation barriers measured on Pt/γ-Al_2O_3 (1.9 nm mean diameter) and Pt powders (400 nm) for temperatures between 423 and 900 K were similar and within experimental uncertainties (15.6 ± 0.1 kJ mol^{-1} and 15.3 ± 0.1 mol^{-1}, respectively), indicating that H_2O-D_2 isotopic exchange rates are not sensitive to the Pt nanoparticle size.[a]

These activation barriers reflect the combined temperature effects of k_6, $\frac{\sqrt{K_3}}{K_5}$, and k_{-5} (eq 2), each with their expected exponential dependences. These combined functional forms, however, do not, in general, lead to a simple exponential dependence for exchange rates described by eq 2; yet, linear trends (on a semilog scale) are evident in Figure 7 for temperatures between 423 and 900 K, suggesting that eq 2 assumes a simpler form throughout this range of temperatures and pressures (40 kPa D_2, 5 kPa H_2O). The value of $\frac{k_6}{k_{-5}}(D_2)$ (0.12 ± 0.074; 473 K) is much smaller than unity, and the H_2O pressure term ((H_2O) = 5 kPa) is small compared to $\frac{\sqrt{K_3}}{K_5}\sqrt{(D_2)}$ (13 ± 3 kPa; 473 K), leading to an approximate form of eq 2

$$-r_{H_2O,f} = r_{HDO,f} + r_{D_2O,f} = \frac{k_6K_5}{\sqrt{K_3}}(H_2O)\sqrt{(D_2)} \tag{5}$$

Therefore, the measured activation barriers (15.6 ± 0.1 kJ; 423−900 K; Pt/γ-Al_2O_3) predominantly reflect the temperature dependence of the $\frac{k_6K_5}{\sqrt{K_3}}$ term (eq 5), thus preserving the strictly exponential trends evident from the date shown in Figure 7.

Above 900 K, exchange rates increase more sensitively with temperature (Figure 7), and the larger apparent barrier (40 ± 0.4 kJ, Pt/γ-Al_2O_3) reflects the emerging contributions from other elementary steps to measured rates.[18,69] This barrier was estimated by extrapolating the rate contributions from low-temperature channels ($D_2-H_2O^*$ and D_2-HDO^*, steps 1.5−1.6, Scheme 1; 423−873 K) and subtracting them from the exchange rates measured at high temperatures (>900 K). This difference was regressed to an Arrhenius functional form to obtain the barrier for these high-temperature channels (87 ± 8 kJ mol^{-1}); these higher values may reflect, in part, contributions from dissociation−recombination routes that contribute to exchange rates, as surfaces become less densely covered at higher temperatures.[37]

H_2O dissociation occurs during water−gas shift reactions on Pt-based catalysts above 500 K.[62−64] H_2O-D_2 exchange may also occur via H_2O dissociation at these higher temperatures to form OH* and H* and then HDO via OH*−D* recombination. The exchange rates as the coverage of bound species decreases with increasing temperature (>900 K)[18,69] are then given by

$$r = k_{dis}K_{H_2O}(H_2O) \tag{6}$$

(derivation in Section SI-4.4.2). In this case, the k_{dis} parameter is the rate constant for H_2O^* dissociation, and K_{H_2O} is the

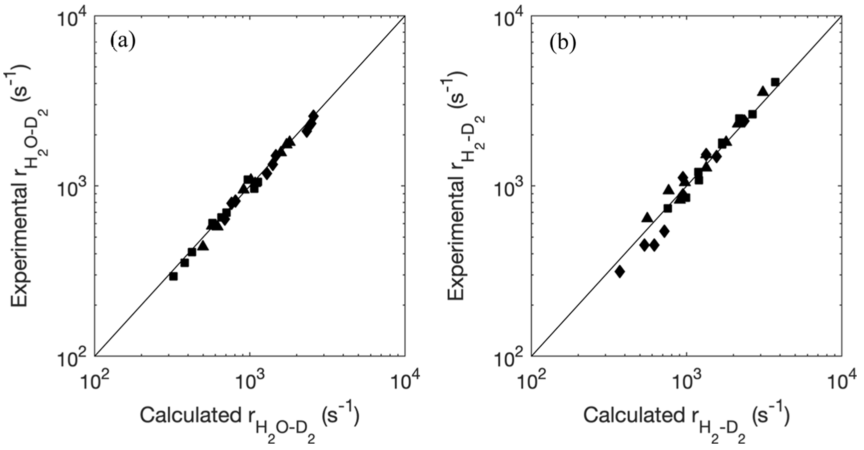

Figure 8. Parity plots of (a) H_2O-D_2 (eq 8) and (b) H_2-D_2 (eq 9) exchange rates in $H_2-D_2-H_2O$ mixtures at (■) 5, (▲) 10, and (◆) 20 kPa of H_2O (H_2O-B) on Pt/γ-Al_2O_3 (473 K). Rates are predicted using kinetic and thermodynamic parameters regressed from independent H_2-D_2[37] and H_2O-D_2 (Section 3.2) isotopic exchange experiments. The additional scatter in H_2-D_2 exchange data is attributed to its calculation through the subtraction of H_2O-D_2 exchange rates from the overall HD formation rates (eq 9).

equilibrium constant for molecular H_2O adsorption. The measured barriers at high temperatures (87 ± 8 kJ mol^{-1}) may therefore reflect the temperature effects on $k_{dis}K_{H_2O}$, which represent, in turn, the energy required to dissociate H_2O on Pt surfaces from a gaseous H_2O molecule; this value resembles those reported for H_2O dissociation on Pt surfaces (Pt(100): 61 kJ mol^{-1} and Pt(111): 75 kJ mol^{-1} at 463 K),[73] suggesting that H_2O-D_2 exchange on Pt occurs via dissociative routes as surfaces become less densely covered at these higher temperatures. These processes become favored over those prevalent on densely covered surfaces at low temperatures; the latter exploit instead the mobility of bound species that become weakly bound at high coverages to avoid the energy penalties imposed by the need to create surface vacancies through recombinative desorption events. These low-temperature routes are mediated by dissociation events of H_2O and D_2 at "spaces" that form locally and momentarily within the dense mobile adlayers that prevail at these low temperatures. Such interpretations are similar to those previously proposed for the evolution of H_2-D_2 isotopic exchange channels with increasing temperature (>900 K).[37]

3.6. H_2-D_2 and H_2O-D_2 Exchange Rates in $H_2O-H_2-D_2$ Mixtures on Pt/γ-Al_2O_3.

H_2-D_2 exchange occurs predominantly via H_2-D^* (and D_2-H^*) associative routes on Pt nanoparticles at temperatures below 700 K under anhydrous conditions;[37] these reaction routes are not expected to change when gaseous ($H_2O(g)$) or bound (H_2O^*) water is also present in the fluid or adlayer phases, respectively. The addition of H_2 to H_2O-D_2 mixtures introduces the additional elementary steps depicted in the second section of Scheme 1. These additional steps include HDO^* and D_2O^* reactions with H_2 to form H_2O^* (step 1.11, Scheme 1) and HDO^* (step 1.12, Scheme 1) (and HD), respectively, as well as those required for H_2-D_2 exchange (steps 1.7−1.10, Scheme 1). Consequently, the rates of HD formation reflect the combined contributions from H_2-D_2 and H_2O-D_2 exchange in $H_2O-H_2-D_2$ mixtures. The proposed elementary steps for the specific H_2-D_2 exchange processes and the kinetic treatment that accurately describes the measured H_2/D_2 exchange were reported previously;[37] they are directly applicable to the description of expressions for H_2-D_2 and H_2O-D_2 isotopic exchange rates when using $H_2O-H_2-D_2$ reactant mixtures.

$H_2O-H_2-D_2$ mixtures form HD molecules through both H_2O-D_2 and H_2-D_2 exchange, leading to HD formation (r_{HD}) and H_2O consumption ($-r_{H_2O} = r_{H_2O-D_2}$) rates (at conditions far from isotopic equilibrium; derivation details in Section SI-5.3) given by

$$r_{HD} = r_{H_2-D_2} + r_{H_2O-D_2} = \frac{2k_4\frac{\sqrt{2K_3}}{K_5}\frac{(H_2)(D_2)}{\sqrt{(H_2)+(D_2)}}\left(1+\frac{k_6}{k_{-5}}(D_2)\right) + k_6(H_2O)(D_2)}{\left((H_2O)+\frac{\sqrt{2K_3}}{K_5}\sqrt{(H_2)+(D_2)}\right)\left(1+\frac{k_6}{k_{-5}}(D_2)\right)} \tag{7}$$

$$r_{H_2O-D_2} = -r_{H_2O} = \frac{k_6(H_2O)(D_2)}{\left((H_2O)+\frac{\sqrt{2K_3}}{K_5}\sqrt{(H_2)+(D_2)}\right)\left(1+\frac{k_6}{k_{-5}}(D_2)\right)} \tag{8}$$

where k_i and K_i correspond to the parameters for each elementary step i in Scheme 1. These equations were obtained for the specific case (applicable here) when exchange rates between water and dihydrogen (steps 1.5−1.6 and 1.11−1.12, Scheme 1; k_6) are much smaller than water desorption rates (reverse of steps 1.2−1.4, Scheme 1; k_{-5}). This case is evidenced in this study by the small values of $\frac{k_6}{k_{-5}}(D_2)$ ratios (0.015−0.06, dimensionless; 10−40 kPa D_2); the value of $\frac{k_6}{k_{-5}}$ ((3.0 ± 1.8) × 10^{-3} kPa^{-1}) was regressed previously from H_2O-D_2 exchange rates (Section 3.2) obtained under conditions that allow for its measurement (2.5−40 kPa H_2O, 5−80 kPa D_2).

The rate of HD formation is given by the sum of H_2O-D_2 and H_2-D_2 exchange pathways (eq 7). The rate of H_2-D_2 exchange can therefore be obtained by subtracting eq 8 from 7 and simplifying to obtain

$$r_{H_2-D_2} = r_{HD} - r_{H_2O-D_2} = \frac{2k_4 \frac{\sqrt{2K_3}}{K_5} \frac{(H_2)(D_2)}{\sqrt{(H_2)+(D_2)}}}{\left((H_2O) + \frac{\sqrt{2K_3}}{K_5}\sqrt{(H_2)+(D_2)}\right)} \quad (9)$$

Equations 7−9 (and the elementary steps in the second section of Scheme 1 for $H_2O-H_2-D_2$ exchange) require only one parameter (k_4) in addition to those already derived from the exchange rates measured with H_2O-D_2 mixtures (k_6, $\frac{\sqrt{K_3}}{K_5}$, and k_{-5}; Section 3.2). This parameter (k_4) is the rate constant for H_2-D_2 exchange via H_2 reactions with D* or D_2 reactions with H* (steps 1.9−1.10, Scheme 1); it is identical for steps 1.9 and 1.10 because these reactions exhibit no detectable kinetic isotope effects.[37] The k_4 value was calculated from H_2-D_2 exchange rates[37] measured on this Pt/γ-Al_2O_3 sample under anhydrous conditions (118 ± 6 kPa^{-1} s^{-1} at 473 K; initial rates in Figure SI-3 and Section SI-3); this value can be used here, together with those of the parameters measured in Section 3.2 ($k_6 = 121 \pm 7$ kPa^{-1} s^{-1}, $\frac{\sqrt{K_3}}{K_5} = 2.1 \pm 0.4$ $kPa^{0.5}$, and $k_{-5} = ((4.0 \pm 2.4) \times 10^4$ $s^{-1})$), to describe H_2O-D_2 (eq 8) and H_2-D_2 (eq 9) exchange rates for $H_2O-H_2-D_2$ mixtures (473 K) if Scheme 1 is applicable for such mixtures without any need to vary the three parameters previously measured in independent experiments. The resulting descriptions do not require the regression of any additional parameters.

H_2-D_2 and H_2O-D_2 exchange rates were measured on Pt/γ-Al_2O_3 at 473 K and a broad range of H_2O (5−20 kPa; H_2O-B), H_2 (5−20 kPa), and D_2 (10−40 kPa) pressures (rate data in Table SI-7 and Section SI-7). The parity plots in Figure 8 show that eqs 8 and 9 accurately describe the rates of H_2-D_2 and H_2O-D_2 isotopic exchange in ternary $H_2O-H_2-D_2$ mixtures without any changes in the elementary steps described in Scheme 1 or in the previously determined magnitudes of their relevant parameters. The proposed kinetic model for H_2O-D_2 isotopic exchange (Scheme 1, first half) brings together the extensive exchange rate data set in earlier sections with the demonstrated mechanism and measured rate parameters for H_2-D_2 exchange under anhydrous conditions[37] (Scheme 1, second half); these two sets of elementary steps occur in parallel but, in contrast with the earlier study,[34] on surfaces that contain kinetically detectable coverages of both H*/D* and H_2O* in the case of $H_2O-H_2-D_2$ mixtures.

3.7. Consequences of Intrapore Liquid Water on HD Formation Rates in $H_2O-H_2-D_2$ Mixtures. The mechanistic framework developed in the previous sections forms the foundation for probing the effects of liquid water on H_2-D_2 and H_2O-D_2 isotopic exchange rates. The results described in this section demonstrate that capillary effects that lead to the formation of a H_2O liquid phase within γ-Al_2O_3 mesopores that contain Pt nanoparticles do not lead to different exchange channels or to $H_2O-H_2-D_2$ exchange rates and kinetic parameters that differ detectably from those in contact with H_2O pressures that do not lead to capillary condensation of a liquid phase.

The individual rates of H_2O-D_2 and H_2-D_2 isotopic exchange (defined as $r_{H_2O-D_2} = -r_{H_2O}$ and $r_{H2-D_2} = r_{HD} - r_{H_2O-D_2}$, respectively) using $H_2-D_2-H_2O$ mixtures were measured on Pt/γ-Al_2O_3 under conditions that cause the condensation of H_2O (323 K) as H_2O (H_2O-B, treated as described in Section 2.3) pressure increases (Figure 9; 20 kPa H_2 and 20 kPa D_2). The H_2O pressure is expressed here as a relative pressure ratio (P/P^{vap}; P^{vap} is the saturation pressure of H_2O at the reaction temperature; 12.3 kPa at 323 K).[74] Figure 9 also depicts the fraction of the γ-Al_2O_3 surface area (and therefore of Pt nanoparticles that reside on such surfaces) that resides within liquid-filled pores as a function of the relative H_2O pressure (Section SI-2), estimated from H_2O uptakes and pore filling calculated using the procedures described in Section 2.4 and in previous studies.[75,76] These estimated H_2O uptake values increase sharply at relative pressures above 0.6−0.7 (Figure 9), indicative of the incipient formation of a H_2O liquid phase within γ-Al_2O_3 voids that are distributed in effective diameter. The condensation of water at similar relative pressures has been demonstrated previously using IR studies at lower temperatures (296 K).[77] The secondary (top) abscissa in Figure 9 shows the mean number of H_2O monolayers at the γ-Al_2O_3 surfaces, calculated using the molal volume and surface tension properties of H_2O and the specific surface area of γ-Al_2O_3.

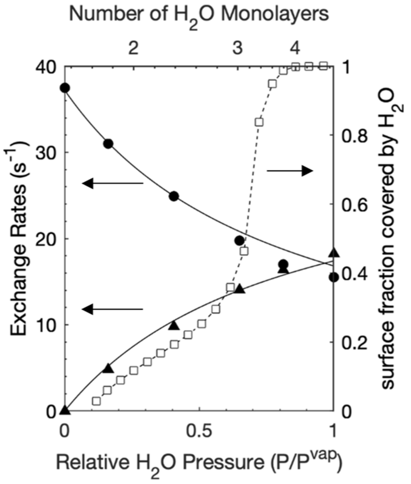

Figure 9. H_2-D_2 (●) and H_2O-D_2 (▲) isotopic exchange rates and surface fraction covered by H_2O (☐) as a function of H_2O pressure (expressed as P/P^{vap}; P^{vap} = 12.3 kPa represents the saturation pressure of H_2O at 323 K) on Pt/γ-Al_2O_3. Solid lines represent model fits (eqs 8 and 9). Dashed line is provided to guide the eye.

The data in Figure 9 show that H_2-D_2 exchange rates decrease and H_2O-D_2 exchange rates increase monotonically (and to a similar extent) with increasing H_2O pressure, without any detectable shift in their kinetics, as the physical state of H_2O evolves from gaseous to physisorbed adlayers to a liquid phase. The solid lines in Figure 9 represent the rates predicted by eqs 8 and 9 using regressed values for k_6, $\frac{\sqrt{K_3}}{K_5}$, k_{-5}, and k_4 (1.6 ± 0.1 kPa^{-1} s^{-1}, 1.1 ± 0.1 $kPa^{0.5}$, $(1.6 \pm 5.1) \times 10^5$, and 1.9 ± 0.2 kPa^{-1} s^{-1}, respectively). Figure 9 shows that the kinetic model derived previously for strictly gaseous reactant mixtures (eq 8-9) with a single value for each parameter (k_6, $\frac{\sqrt{K_3}}{K_5}$, k_{-5}, and k_4) is able to describe rates in the absence or presence of an intrapore liquid phase. These values cannot be compared numerically to those reported above (Section 3.3; 473 K) because of the lower temperatures (323 K) required to enable the formation of liquid H_2O at ambient reactor pressures; nevertheless, the agreement obtained with param-

Scheme 2. Thermodynamic Cycle Showing H_2−D_2 Exchange (and Its Relevant TS) in the Absence (Top) and Presence (Bottom) of Liquid H_2O[a]

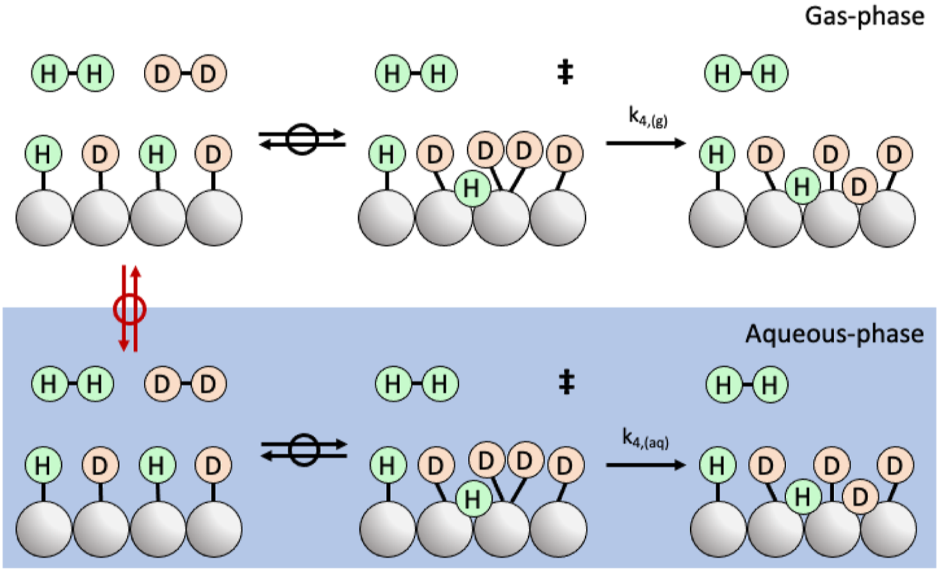

[a] All reactants in the gaseous and aqueous (solvated) phases (and therefore also the TS) are quasi-equilibrated.

eters that remain unchanged upon the formation of a contacting liquid phase indicates that the liquid phase does not introduce detectable changes in any of the kinetic or thermodynamic parameters required to describe the dynamics of H_2−D_2 or H_2O−D_2 exchange (Figure 9).

Next, we address the matters of when, how, and why a contacting liquid phase would influence reaction rates on surfaces with isotopic exchange processes and liquid H_2O as illustrative examples. The effects of liquid H_2O (or their absence) on H_2−D_2 and H_2O−D_2 isotopic exchange rates in Figure 9 must be addressed by considering the plausible solvation of TSs by a liquid in the context of nonideal thermodynamic treatments of chemical dynamics. Turnover rates and selectivities can be influenced by changes in the outer sphere environment of the TS induced by a liquid, as previously demonstrated in the case of nonpolar liquids for aldol condensation[56] and alkene dimerization[55,78] reactions.

Liquid H_2O provides a dense polar environment that may be able to stabilize (or destabilize) TSs and bound intermediates, particularly those involving charge-transfer processes or ionic species.[79−81] The magnitude of such effects depends on the extent to which the TS is stabilized by its direct coordination to binding sites (inner sphere) instead of that through interactions with the liquid environment (outer sphere). The consequences of solvation effects on reactivity are therefore most evident when kinetically relevant steps involve adsorption (entry) or desorption (exit) steps because the bonds with the surface remain incomplete at the respective TSs for these elementary events.[56,82]

Transition state theory postulates a quasi-equilibrium between the activated complex (TS) and its reactants in each elementary step, leading to rate constants given by

$$k = \frac{k_B T}{h} a^{\ddagger} = \frac{k_B T}{h} K^{\ddagger} \frac{1}{\gamma^{\ddagger}} = \frac{k_B T}{h} e^{-\Delta G^{\ddagger}/RT} \tag{10}$$

where k_B is the Boltzmann constant, T is the absolute temperature, h is Planck's constant, $a^{\ddagger}$ denotes the thermodynamic activity of the TS, $K^{\ddagger}$ is the thermodynamic constant for the hypothesized equilibration between the activated complex and the reactants, $\gamma^{\ddagger}$ is the activity coefficient of the TS, and $\Delta G^{\ddagger}$ represents the Gibbs free energy of activation; the latter includes a term, typically denoted as excess free energy, which accounts for specific solvation of the TS (the $\gamma^{\ddagger}$ term). Such treatments of rate constants remain applicable when reactions occur in the presence of a contacting aqueous phase. When species i in the aqueous and gaseous phases are in vapor−liquid equilibrium (i.e., in the absence of diffusional effects), their chemical potentials are identical in the two phases ($\mu_{i,(aq)} = \mu_{i,(g)}$), as is also the case for their thermodynamic activities $a_{i,(aq)} = a_{i,(g)}$, or equivalently fugacities, $f_{i,(aq)} = f_{i,(g)}$, using the same standard state for both phases. Eq 10, with rate constants (k) defined in terms of the pressure of gaseous reactants in equilibrium with the liquid phase, can then be used to describe rates in the presence of liquid H_2O, as long as the species in the liquid and gas phases are in equilibrium.[83] The ratio of rates in the presence and absence of liquid H_2O is then given by

$$\frac{r_{(aq)}}{r_{(g)}} = \frac{k_{(aq)}}{k_{(g)}} = \frac{a^{\ddagger}_{(aq)}}{a^{\ddagger}_{(g)}} = \frac{\gamma^{\ddagger}_{(g)}}{\gamma^{\ddagger}_{(aq)}} = e^{-\Delta\Delta G^{\ddagger}/RT} \tag{11}$$

where $\Delta\Delta G^{\ddagger}$ is the difference in Gibbs free energy of activation (referenced to gaseous reactants) between the reaction in the aqueous phase and that in the gas phase

$$\begin{aligned} \Delta\Delta G^{\ddagger} &= \Delta G^{\ddagger}_{(aq)} - \Delta G^{\ddagger}_{(g)} = \\ &(G^{E}_{TS,(aq)} - G_{TS,ideal} - G_{reactants}) \\ &\quad - (G^{E}_{TS,(g)} - G_{TS,ideal} - G_{reactants}) = \\ &G^{E}_{TS,(aq)} - G^{E}_{TS,(g)} \end{aligned} \tag{12}$$

where G^E represents the excess Gibbs free energy. Eqs 11 and 12 show that differences in rates arising from the presence of a contacting dense phase reflect the differences in the Gibbs free

Scheme 3. Reaction Coordinate Diagram for H_2−D_2 Exchange on Pt when the Contacting Fluid Phase is Gaseous (Dashed Black Lines) and when It is Liquid Water (Dotted Blue Lines)[a]

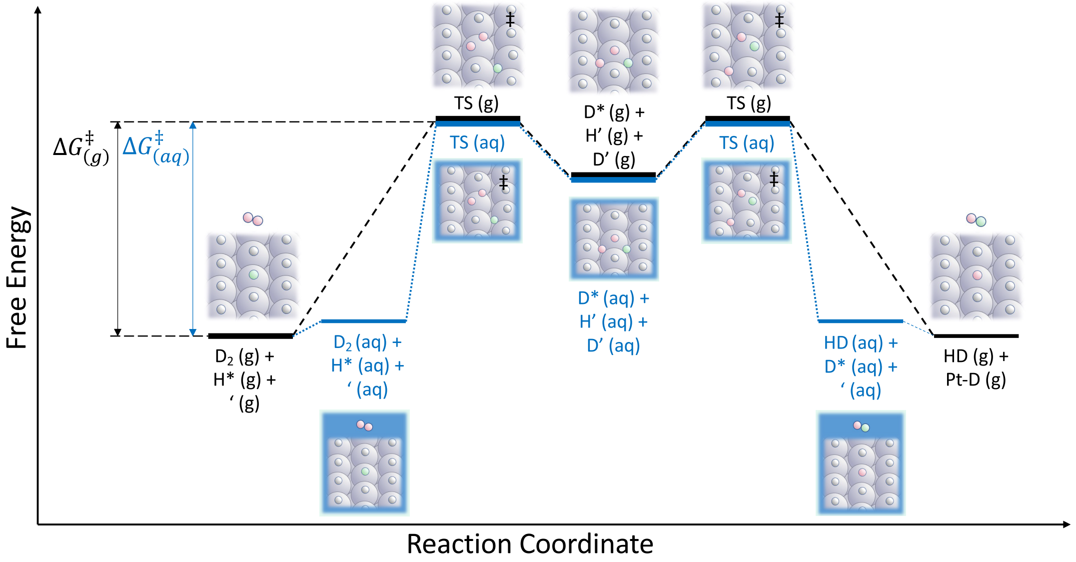

[a]Deuterium atoms involved in the isotopic exchange are shown as red spheres and hydrogen atoms as green spheres. The TS structures are reproduced from our previous study and are denoted by ‡.[37]

energy of activation $\Delta\Delta G^{\ddagger}$, specifically the excess free energy of the TS ($G_{TS}{}^{E}$; eq 12), and the concomitant differences in the activity coefficients of the TS

$$G^{E}_{TS,(aq)} - G^{E}_{TS,(g)} = RT\ln(\gamma^{\ddagger}_{(aq)}) - RT\ln(\gamma^{\ddagger}_{(g)}) \quad (13)$$

These concepts are next used to interpret the absence of consequences of liquid water on H_2−D_2 and H_2O−D_2 isotopic exchange rates in H_2−D_2−H_2O mixtures (Figure 9).

Our previous study demonstrated that H_2−D_2 exchange channels on Pt surfaces saturated with H*/D* adlayers involve the dissociative adsorption of H_2 (or D_2) at "landing" spaces made available by the local displacements of mobile H* or D* adatoms (atop) to alternate (fcc) binding sites on the Pt surface (denoted as ')[37]

$$D_2 + H^* + ' \xrightarrow{k_4} H' + D^* + D' \quad (14)$$

This elementary step (and its TS; Scheme 2 (top)) also describes events in which H_2 exchanges with D* with similar rates in eq 14 because of negligible kinetic isotope effects.[37] The dashed black pathway in Scheme 3 depicts the reaction coordinate diagram for this reaction with purely gaseous reactants; the rate constant $k_{4,(g)}$ reflects the difference in Gibbs free energy between the TS and the reactants (H_2(g), D*(g), and '(g)) in the absence of a solvating liquid (denoted by $\Delta G_{(g)}{}^{\ddagger}$; Scheme 3, dashed black pathway).

The data shown in Figure 9 indicate that H_2−D_2 isotopic exchange is mediated by the same TS (Scheme 2 (bottom) and Scheme 3 (dotted blue lines)), albeit one being possibly different in stability, whether an aqueous liquid phase is present or not. The rate constant for the reaction in the presence of the liquid phase ($k_{4,(aq)}$; Scheme 2 (bottom)) reflects the free energy of activation for the surface-bound TS in contact with liquid water ($\Delta G_{(aq)}{}^{\ddagger}$; Scheme 3 (dotted blue lines)). The dissolution of gaseous species in liquid H_2O is quasi-equilibrated under conditions of vapor−liquid equilibrium. The H* and D* coverages are set by quasi-equilibrated dissociative adsorption of H_2 and D_2,[37] leading to equilibration among gaseous reactants, solvated reactants, and their respective bound species (denoted by red equilibrium reaction arrows, ⇄, in Scheme 2). Schemes 2 and 3, taken together, consider that (in the absence of diffusional restrictions, leading to local chemical potential gradients) $\Delta\Delta G^{\ddagger}$ values merely reflect the effects of the solvent on the excess free energy (or activity coefficient) of the TS (eqs 12 and 13). In the absence of such solvating effects, $\Delta\Delta G^{\ddagger}$ is zero (eq 12), and $\gamma_{(g)}{}^{\ddagger}$ and $\gamma_{(aq)}{}^{\ddagger}$ are identical (eq 13), thus precluding any consequence of liquid water on isotopic exchange rates. These concepts, illustrated here for H_2−D_2 exchange reactions, also apply to H_2O−D_2 exchange

$$D_2 + H_2O^* + ' \xrightarrow{k_6} H_2O' + D^* + D' \quad (15)$$

and the relevant rate parameters for the unsolvated ($k_{6,(g)}$) and solvated ($k_{6,(aq)}$) systems.

H_2−D_2 exchange rates in the presence of H_2O(g) are accurately described by eq 9 (Section 3.4); this equation accounts for competitive adsorption of H_2O^* (step 1.2, Scheme 1) on Pt surfaces, whether such surfaces are in contact with liquid water or not. Rates of H_2−D_2 exchange reactions in the aqueous phase (assuming the same reaction pathway as in the absence of a liquid phase; Schemes 2 and 3) are described by

$$r_{H_2-D_2} = \frac{2k_{4,(aq)}\frac{\sqrt{2K_{3,(aq)}}}{K_{5,(aq)}}\frac{(H_2)(D_2)}{\sqrt{(H_2)+(D_2)}}}{\left((H_2O) + \frac{\sqrt{2K_{3,(aq)}}}{K_{5,(aq)}}\sqrt{(H_2) + (D_2)}\right)} \quad (16)$$

The (aq) subscript in this equation denotes equilibrium and rate constants when liquid water is present. Similarly, H_2O−D_2 exchange rates in gas-phase H_2−D_2−H_2O mixtures are described by eq 8, while rates in the presence of liquid H_2O are given by

$$r_{H_2O-D_2} = -r_{H_2O} = \frac{k_{6,(aq)}(H_2O)(D_2)}{\left((H_2O) + \frac{\sqrt{2K_{3,(aq)}}}{K_{5,(aq)}}\sqrt{(H_2) + (D_2)}\right)\left(1 + \frac{k_{6,(aq)}}{k_{-5,(aq)}}(D_2)\right)} \tag{17}$$

It is evident when comparing eqs 16 and 17 to 9 and 8, respectively, that three rate constant ratios ($\frac{k_{4,(aq)}}{k_{4,(g)}}$, $\frac{k_{6,(aq)}}{k_{6,(g)}}$, $\frac{k_{-5,(aq)}}{k_{-5,(g)}}$; eq 11) and one equilibrium constant ratio ($\frac{\sqrt{K_{3,(aq)}}}{K_{5,(aq)}} / \frac{\sqrt{K_{3,(g)}}}{K_{5,(g)}}$) may plausibly differ from unity, reflecting changes in activity coefficients (eq 11) and thus informing about the consequences of a liquid H_2O outer sphere on the surface-mediated exchange process of interest in this study.

The value of $\frac{k_{4,(aq)}}{k_{4,(g)}}$ reflects differences in the excess free energy ($\Delta\Delta G^{\ddagger}$; eqs 11 and 12) and activity coefficients ($\gamma^{\ddagger}$; eq 13) of the TS for H_2−D_2 exchange in the presence and absence of a liquid, referenced to the gaseous reactants. These TSs are identical, except for possible interactions between the incoming H_2 (or D_2) molecule and the surrounding liquid. H_2(g) is only weakly solvated by liquid water ($\Delta H_{diss} = -3.2$ kJ mol^{-1}; 273−303 K);[84] the effects of liquid water on H_2 in the TS are also, therefore, expected to be weak. Our previous study also showed that this TS interacts with Pt surfaces through each of its three hydrogen atoms and closely resembles the bound intermediate ($D^* + H' + D'$; Scheme 3).[37] The "late" TS thus exhibits nearly complete bonds with the surface and differs from other reactions for which the effects of liquids have been observed;[55,56,78] these latter reactions exhibited "early" or "late" structures for entry and exit steps, respectively, and thus less complete bonds with the catalyst surface at their respective TSs, allowing for more interactions with the outer-sphere environment. The TS for H_2−D_2 exchange is thus expected to be stabilized primarily by interactions with the Pt surfaces and weakly influenced by the presence of liquid H_2O, resulting in nearly identical activity coefficients ($\gamma_{(g)}^{\ddagger}$ vs $\gamma_{(aq)}^{\ddagger}$; eq 13) and a $\Delta\Delta G^{\ddagger}$ value near zero (eqs 12 and 13). This absence of solvation effects leads to a $\frac{k_{4,(aq)}}{k_{4,(g)}}$ ratio near unity (eq 12). The parameter k_6 is the rate constant for the reaction between D_2 and H_2O^* (steps 1.5 and 1.6, Scheme 1). This elementary step is proposed to proceed via a nearly identical TS as for the reaction of D_2 and H^* (eq 14), making the arguments for the effects of liquid water on $\frac{k_{4,(aq)}}{k_{4,(g)}}$ and $\frac{k_{6,(aq)}}{k_{6,(g)}}$ ratios identical.

The $\frac{\sqrt{K_{3,(g)}}}{K_{5,(g)}}$ (and $\frac{\sqrt{K_{3,(aq)}}}{K_{5,(aq)}}$) terms represent the ratios of equilibrium constants for H_2 (or D_2) dissociative chemisorption (K_3) and H_2O molecular adsorption (K_5). These equilibrium constants can be defined rigorously using the thermodynamic activities of all species involved

$$K_3 = \frac{a_{H*}^2}{a_{H_2}a_*^2} \tag{18}$$

$$K_5 = \frac{a_{H_2O*}}{a_{H_2O}a_*} \tag{19}$$

As discussed above, all species in their gaseous (unsolvated) state (H_2(g), D_2(g), H^*(g), D^*(g), H_2O^*(g), and $*$(g)) are in equilibrium with their solvated counterparts (H_2(aq), D_2(aq), H^*(aq), D^*(aq), H_2O^*(aq), and $*$(aq)); consequently, their chemical potentials and thermodynamic activities are identical in their two states to the extent that these intermediates are stabilized by direct coordination with the binding site (inner sphere). Molecularly bound H_2O^* is plausibly stabilized by the presence of liquid water. Several studies have shown, however, that adsorbed water on Pt(111) exhibits surprising "hydrophobic" qualities and only weak hydrogen-bonding interactions (<6 kJ mol^{-1}) compared to interactions with the surface (−51.3 ± 1.6 kJ mol^{-1}, 0.5 ML H_2O).[67,68] K_3 and K_5 values are therefore expected to be only weakly affected by the nature or density of the contacting fluid phase, leading to $\frac{\sqrt{K_{3,(aq)}}}{K_{5,(aq)}} / \frac{\sqrt{K_{3,(g)}}}{K_{5,(g)}}$ ratios near unity.

The $\frac{k_{-5,(aq)}}{k_{-5,(g)}}$ ratio reflects the difference in excess Gibbs free energy of the TS (eqs 11 and 12) for the desorption of water molecules (steps 1.2−1.4, Scheme 1) between Pt nanoparticles in contact with a liquid and those in contact with gaseous phases. It is this ratio that may seem most plausibly different from unity because H_2O molecules in the dense liquid phase can make more H-bonding "contacts" with surface H_2O molecules and with their desorption TS.[85,86] Such dense protic environments could stabilize the desorption TS (steps 1.2−1.4, Scheme 1; an exit step) and increase desorption rates (leading to $\frac{k_{-5,(aq)}}{k_{-5(g)}} > 1$; eqs 11 and 12), and to a smaller $\frac{k_{6,(aq)}}{k_{-5,(aq)}}$ value (eq 17), when liquid water is present. The regressed values of the $\frac{k_6}{k_{-5}}(D_2)$ term in eq 8 are, however, much smaller than unity and weakly influence the measured rates, even in the absence of a liquid phase (0.12 ± 0.074, Section 3.2). Its even smaller value when a liquid is present would make its contribution to the measured H_2O−D_2 exchange rates less consequential.

These inferences about the relevant ratios of rate and equilibrium constants ($\frac{k_{4,(aq)}}{k_{4,(g)}}$, $\frac{k_{6,(aq)}}{k_{6,(g)}}$, $\frac{k_{-5,(aq)}}{k_{-5,(g)}}$, and $\frac{\sqrt{K_{3,(aq)}}}{K_{5,(aq)}} / \frac{\sqrt{K_{3,(g)}}}{K_{5,(g)}}$) and the absence of detectable consequences of solvation for H_2−D_2 and H_2O−D_2 exchange rates are supported by our experimental data (Figure 9) and our mechanistic framework for their analysis. The formation of a H_2O liquid phase within Pt/γ-Al_2O_3 mesopores does not detectably influence exchange rates, kinetic trends, or rate and equilibrium constants, which remain the same as those on nanoparticles in contact with a strictly gaseous phase. These findings show that the effects of liquid H_2O on H_2−D_2 and H_2O−D_2 exchange are too weak to be detected experimentally, in contrast with other reactions for which such effects are reported (e.g., CH_4 activation and polyol reforming).[54,87,88] They also challenge the conclusions of previous studies[34] that attribute the consequences of a liquid water phase for H_2−D_2 exchange rates to significant changes in the electronic properties of metals placed in contact with liquid water;[34,51−53] these effects were, in turn, proposed to reflect a large decrease in the binding strength and stability of H^* and D^* intermediates.[34,54] Our study demonstrates that (1) the mechanism of exchange is unaffected by the physical form of water (gas or liquid) in contact with the catalyst (only the chemical potential of H_2O influences rates—it is identical when the gas and liquid phases are in equilibrium), (2) the TSs for H_2−D_2 exchange on densely covered surfaces in contact with gas phase or liquid H_2O are in equilibrium with one another, (3) H_2−D_2 (and H_2O−D_2) exchange rates are not able to detect any preferential (de)stabilization of H* and D* intermediates because they report only the free-energy barrier between the TS and a densely covered surface in the gas phase (Scheme 3), and (4) H_2−D_2 (and H_2O−D_2) exchange rates do not detect changes in the combined effects of liquid H_2O on the binding of the TS (inner sphere) nor its solvation (outer sphere).

The present study remains silent about the binding of reactive intermediates (e.g., H*, D*, and H_2O*) and their respective adsorption equilibrium constants. These effects of a contacting liquid phase on binding energy, if they were present, would only influence adsorption equilibrium constants in the $\frac{\sqrt{K_3}}{K_5}$ term (eqs 8 and 9) but not H_2−D_2 exchange rates, which are shown to be insensitive to this term in thermodynamic analysis described above. Changes in rates or kinetic trends resulting from the presence of a liquid would require the (de)stabilization of the TS for kinetically relevant elementary steps with concomitant consequences for their activation free energies (eqs 11 and 12; Scheme 3). Thus, H_2−D_2 and D_2−H_2O exchange rates cannot be used to posit any effects of water on the binding of chemisorbed hydrogen. Such information may be obtainable via theoretical calculations (e.g., ab initio molecular dynamics and DFT) that are beyond the scope of our present work but which must be benchmarked for accuracy against our measured rates and their kinetic trends. The experimental data, kinetic trends, and mechanistic assessment presented here, however, stand independently of any theoretical calculations and of any effects of liquid H_2O on the binding properties of intermediates. This study shows that H_2O−D_2 and H_2−D_2 isotopic exchange kinetics in liquid H_2O reflect the prevailing chemical potentials (or fugacities) of gas-phase H_2, D_2, and H_2O in equilibrium with their solvated counterparts. The effects of H_2O pressure on H_2−D_2 and H_2O−D_2 exchange rates merely reflect the relative coverages of species derived from H_2O, D_2, and H_2 at their respective contacting pressures. While liquid water may indeed affect the work function of metal surfaces, this merely reflects the stabilization of the ejected electron in liquid water (the electron affinity of water, 0.1−0.3 eV)[89−91] and not changes in the electronic properties of either bulk metals or, in this case, Pt nanoparticles.

4. CONCLUSIONS

This study rigorously addressed the underlying kinetics of H_2O−D_2 and H_2−D_2 isotopic exchange reactions in both gas- and liquid-phase environments. H_2O−D_2 exchange was shown to occur in the gas phase via the dissociative adsorption of D_2 and subsequent reaction of chemisorbed D* (at alternative binding modes) with competitively bound H_2O*. Such a pathway was shown to be applicable for a wide range of temperatures (up to approximately 900 K) and is reminiscent of our previous work on H_2−D_2 exchange. The kinetic model for H_2O−D_2 exchange was further shown to be compatible with our prior H_2−D_2 exchange model and predictive of H_2−D_2 and H_2O−D_2 exchange rates in ternary gas phase H_2O−H_2−D_2 mixtures. The model was then used to probe how changes in the outer-sphere environment affect exchange rates by inducing the formation of a H_2O liquid phase within Pt/γ-Al_2O_3 mesopores. H_2−D_2 and H_2O−D_2 exchange rates did not deviate from the gas-phase model even as the catalyst pores were filled, indicating the absence of strong liquid H_2O solvation effects. These results reflect the predominant stabilization of TSs by the inner-sphere environment (i.e., Pt surface) for these reactions. The rigorous insights obtained in this study were possible only after extensive purification and degassing of reactant H_2O, which otherwise lead to irreversible and confounding titration artifacts. The implications of these results are important for a wide variety of aqueous catalytic processes and provide a framework for rigorously utilizing and interpreting H−D exchange kinetic data in future studies.

■ ASSOCIATED CONTENT

Supporting Information

The Supporting Information is available free of charge at https://pubs.acs.org/doi/10.1021/acs.jpcc.3c04678.

> Supporting calculations used in methods; N_2 adsorption isotherms on γ-Al_2O_3; effects of CO_2 contamination on H_2−D_2 exchange rates; rate equations and kinetic analysis of alternative H_2O−D_2 exchange mechanisms; derivation of rate equations for H_2O−D_2 and H_2O−H_2−D_2 exchange mediated by reactions of D_2 and H_2O*; sensitivity analysis of k_6, $\frac{\sqrt{K_3}}{K_5}$, and k_{-5} and parity plots for H_2O−D_2 exchange; and H_2−D_2 and H_2O−D_2 isotopic exchange rates in H_2O−H_2−D_2 mixtures (PDF)

■ AUTHOR INFORMATION

Corresponding Author

Enrique Iglesia − *Department of Chemical Engineering, University of California at Berkeley, Berkeley, California 94720, United States;* orcid.org/0000-0003-4109-1001; Phone: (510) 642-9673; Email: iglesia@cchem.berkeley.edu; Fax: (510) 642-4778

Authors

Samuel L. Leung − *Department of Chemical Engineering, University of California at Berkeley, Berkeley, California 94720, United States;* orcid.org/0000-0002-0915-1361

Sai Chen − *Department of Chemical Engineering, University of California at Berkeley, Berkeley, California 94720, United States;* Present Address: School of Chemical Engineering & Technology Tianjin University, Tianjin 300354, People's Republic of China

Complete contact information is available at: https://pubs.acs.org/10.1021/acs.jpcc.3c04678

Notes

The authors declare no competing financial interest.

■ ACKNOWLEDGMENTS

This study was funded by Chevron Corporation. S.L.L. acknowledges funding from a Chevron Graduate Student Research Fellowship.

■ ADDITIONAL NOTE

[a] As discussed in Section [2.3], turnover rates could not be calculated directly for Pt powders because of uncertain surface areas, but comparisons of temperature sensitivity among samples do not require that rates be normalized by the amount of exposed surfaces.

■ REFERENCES

(1) Fogler, H. S. *Elements of Chemical Reaction Engineering*, 4th ed.; Prentice Hall PTR: Upper Saddle River, NJ, 2006; p 1080.

(2) Christmann, K. Interaction of Hydrogen with Solid-Surfaces. *Surf. Sci. Rep.* **1988**, *9*, 1−163.

(3) Cardonamartinez, N.; Dumesic, J. A. Applications of Adsorption Microcalorimetry to the Study of Heterogeneous Catalysis. *Adv. Catal.* **1992**, *38*, 149−244.

(4) Dumesic, J. A.; Rudd, D. F.; Aparicio, L. M.; Rekoske, J. E.; Treviño, A. A. *Microkinetics of Heterogeneous Catalysis*; American Chemical Society: Washington, DC, 1993; p 316.

(5) Flaherty, D. W.; Hibbitts, D. D.; Gurbuz, E. I.; Iglesia, E. Theoretical and kinetic assessment of the mechanism of ethane hydrogenolysis on metal surfaces saturated with chemisorbed hydrogen. *J. Catal.* **2014**, *311*, 350−356.

(6) Sinfelt, J. H. Specificity in Catalytic Hydrogenolysis by Metals. In *Adv. Catal.*; Eley, D. D., Pines, H., Weisz, P. B., Eds.; Academic Press, 1973; Vol. *23*, pp 91−119.

(7) Sinfelt, J. H.; Yates, D. J. C.; Carter, J. L. Catalytic Hydrogenolysis and Dehydrogenation over Copper-Nickel Alloys. *J. Catal.* **1972**, *24*, 283−296.

(8) Zhang, Q. W.; Li, J.; Liu, X. X.; Zhu, Q. M. Synergetic effect of Pd and Ag dispersed on Al2O3 in the selective hydrogenation of acetylene. *Appl. Catal., A* **2000**, *197*, 221−228.

(9) Spielmann, J.; Buch, F.; Harder, S. Early Main-Group Metal Catalysts for the Hydrogenation of Alkenes with H-2. *Angew. Chem., Int. Ed.* **2008**, *47*, 9434−9438.

(10) Sermon, P. A.; Bond, G. C.; Wells, P. B. Hydrogenation of Alkenes over Supported Gold. *J. Chem. Soc., Faraday Trans. 1* **1979**, *75*, 385−394.

(11) Chupin, J.; Gnep, N. S.; Lacombe, S.; Guisnet, M. Influence of the metal and of the support on the activity and stability of bifunctional catalysts for toluene hydrogenation. *Appl. Catal., A* **2001**, *206*, 43−56.

(12) Basset, J. M.; Dalmaiimelik, G.; Primet, M.; Mutin, R. A study of benzene hydrogenation and identification of the adsorbed species with Pt/Al2O3 catalysts. *J. Catal.* **1975**, *37*, 22−36.

(13) Lin, S. D.; Vannice, M. A. Hydrogenation of Aromatic Hydrocarbons over Supported Pt Catalysts .II. Toluene Hydrogenation. *J. Catal.* **1993**, *143*, 554−562.

(14) Boccuzzi, F.; Chiorino, A.; Manzoli, M.; Andreeva, D.; Tabakova, T. FTIR study of the low-temperature water-gas shift reaction on Au/Fe2O3 and Au/TiO2 catalysts. *J. Catal.* **1999**, *188*, 176−185.

(15) Iruretagoyena, D.; Hellgardt, K.; Chadwick, D. Towards autothermal hydrogen production by sorption-enhanced water gas shift and methanol reforming: A thermodynamic analysis. *Int. J. Hydrogen Energy* **2018**, *43*, 4211−4222.

(16) Ernst, K.-H.; Campbell, C. T.; Moretti, G. Kinetics of the Reverse Water Gas Shift Reaction over Cu(110). *J. Catal.* **1992**, *134*, 66−74.

(17) Zhang, C. H.; Zhao, G. Y.; Liu, K. K.; Yang, Y.; Xiang, H. W.; Li, Y. W. Adsorption and reaction of CO and hydrogen on iron-based Fischer−Tropsch synthesis catalysts. *J. Mol. Catal. A: Chem.* **2010**, *328*, 35−43.

(18) Garcia-Dieguez, M.; Hibbitts, D. D.; Iglesia, E. Hydrogen Chemisorption Isotherms on Platinum Particles at Catalytic Temperatures: Langmuir and Two-Dimensional Gas Models Revisited. *J. Phys. Chem. C* **2019**, *123*, 8447−8462.

(19) Candy, J.-P.; Fouilloux, P.; Renouprez, A. J. Hydrogen Adsorption on Platinum Catalysts-Quantitative-Determination of the Various Species Population. *J. Chem. Soc., Faraday Trans. 1* **1980**, *76*, 616−629.

(20) Norton, P. R.; Richards, P. J. The heat of adsorption of hydrogen on platinum. *Surf. Sci.* **1974**, *44*, 129−140.

(21) Vannice, M. A.; Hasselbring, L. C.; Sen, B. Direct measurements of heats of adsorption on platinum catalysts I. H2 on Pt dispersed on SiO2, Al2O3, SiO2$z.sbnd;Al2O3, and TiO2. *J. Catal.* **1985**, *95*, 57−70.

(22) Vannice, M. A.; Hasselbring, L. C.; Sen, B. Metal-support effects on hydrogen and carbon monoxide heats of adsorption on titania-supported platinum. *J. Phys. Chem.* **1985**, *89*, 2972−2973.

(23) Kunimatsu, K.; Senzaki, T.; Tsushima, M.; Osawa, M. A combined surface-enhanced infrared and electrochemical kinetics study of hydrogen adsorption and evolution on a Pt electrode. *Chem. Phys. Lett.* **2005**, *401*, 451−454.

(24) Nichols, R. J.; Bewick, A. Spectroscopic Identification of the Adsorbed Intermediate in Hydrogen Evolution on Platinum. *J. Electroanal. Chem.* **1988**, *243*, 445−453.

(25) Clavilier, J.; Armand, D. Electrochemical induction of changes in the distribution of the hydrogen adsorption states on Pt (100) and Pt (111) surfaces in contact with sulphuric acid solution. *J. Electroanal. Chem.* **1986**, *199*, 187−200.

(26) Conway, B. E.; Jerkiewicz, G. Thermodynamic and Electrode Kinetic Factors in Cathodic Hydrogen Sorption into Metals and Its Relationship to Hydrogen Adsorption and Poisoning. *J. Electroanal. Chem.* **1993**, *357*, 47−66.

(27) Gomez, R.; Orts, J. M.; Alvarez-Ruiz, B.; Feliu, J. M. Effect of temperature on hydrogen adsorption on Pt(111), Pt(110), and Pt(100) electrodes in 0.1 M HClO4. *J. Phys. Chem. B* **2004**, *108*, 228−238.

(28) Gomez-Marin, A. M.; Feliu, J. M. Thermodynamic properties of hydrogen-water adsorption at terraces and steps of Pt(111) vicinal surface electrodes. *Surf. Sci.* **2016**, *646*, 269−281.

(29) Christmann, K.; Ertl, G.; Pignet, T. Adsorption of Hydrogen on a Pt(111) Surface. *Surf. Sci.* **1976**, *54*, 365−392.

(30) Koeleman, B. J. J.; Dezwart, S. T.; Boers, A. L.; Poelsema, B.; Verhey, L. K. Adsorption Study of Hydrogen on a Stepped Pt (997) Surface Using Low-Energy Recoil Scattering. *Nucl. Instrum. Methods Phys. Res.* **1983**, *218*, 225−229.

(31) Chen, X. T.; McCrum, I. T.; Schwarz, K. A.; Janik, M. J.; Koper, M. T. M. Co-adsorption of Cations as the Cause of the Apparent pH Dependence of Hydrogen Adsorption on a Stepped Platinum Single-Crystal Electrode. *Angew. Chem., Int. Ed.* **2017**, *56*, 15025−15029.

(32) Almithn, A.; Hibbitts, D. Effects of Catalyst Model and High Adsorbate Coverages in ab Initio Studies of Alkane Hydrogenolysis. *ACS Catal.* **2018**, *8*, 6375−6387.

(33) Almithn, A. S.; Hibbitts, D. D. Supra-Monolayer Coverages on Small Metal Clusters and Their Effects on H-2 Chemisorption Particle Size Estimates. *AIChE J.* **2018**, *64*, 3109−3120.

(34) Yang, G. J.; Akhade, S. A.; Chen, X.; Liu, Y.; Lee, M. S.; Glezakou, V. A.; Rousseau, R.; Lercher, J. A. The Nature of Hydrogen Adsorption on Platinum in the Aqueous Phase. *Angew. Chem., Int. Ed.* **2019**, *58*, 3527−3532.

(35) Amenomiya, Y. Adsorption of Hydrogen and H2-D2 Exchange Reaction on Alumina. *J. Catal.* **1971**, *22*, 109−122.

(36) Enyo, M. Isotope Exchange and Equilibration Reaction on Nickel in the System Deuterium-Light Water. *J. Res. Inst. Catal. Hokkaido Univ.* **1967**, *15*, 1−20.

(37) Leung, S. L.; Hibbitts, D.; Gárcia-Diéguez, M.; Iglesia, E. Binding and Exchange Reactions of Hydrogen Isotopes on Surfaces of Dispersed Pt Nanoparticles. *J. Phys. Chem. C* **2022**, *126*, 3923−3938.

(38) Nieuwenhuys, B. E. Influence of the surface structure on the adsorption of hydrogen on platinum, as studied by field emission probe-hole microscopy. *Surf. Sci.* **1976**, *59*, 430−446.

(39) Poelsema, B.; Lenz, K.; Comsa, G. The dissociative adsorption of hydrogen on defect-'free' Pt(111). *J. Phys.: Condens. Matter* **2010**, *22*, 304006.

(40) Christmann, K. Adsorption of Hydrogen on a Nickel (100) Surface. *Z. Naturforsch., A: Phys. Sci.* **1979**, *34*, 22−29.

(41) Koningsberger, D. C.; Oudenhuijzen, M. K.; de Graaf, J.; van Bokhoven, J.; Ramaker, D. E. In situ X-ray absorption spectroscopy as a unique tool for obtaining information on hydrogen binding sites and electronic structure of supported Pt catalysts: towards an understanding of the compensation relation in alkane hydrogenolysis. *J. Catal.* **2003**, *216*, 178−191.

(42) Avgouropoulos, G.; Ioannides, T. CO tolerance of Pt and Rh catalysts: effect of CO in the gas-phase oxidation of H-2 over Pt and Rh supported catalysts. *Appl. Catal., B* **2005**, *56*, 77−86.

(43) Schreier, M.; Yoon, Y.; Jackson, M. N.; Surendranath, Y. Competition between H and CO for Active Sites Governs Copper-

Mediated Electrosynthesis of Hydrocarbon Fuels. *Angew. Chem., Int. Ed.* **2018**, *57*, 10221−10225.

(44) Miyamoto, S.; Sakka, T.; Iwasaki, M. Hydrogen Isotope Exchange between D2 and H2o Catalyzed by Platinum Plate. *Can. J. Chem.* **1989**, *67*, 857−861.

(45) Kawakami, K.; Takao, Y.; Kusunoki, K. Kinetics of Isotopic Exchange-Reaction between Hydrogen and Water-Vapor over Platinum Supported on a Hydrophobic Carrier. *Can. J. Chem. Eng.* **1986**, *64*, 432−439.

(46) Knoche, W. *Chemical Reactions of CO_2 in Water*; Springer: Berlin, Heidelberg, 1980; pp 3−11.

(47) Carroll, J. J.; Slupsky, J. D.; Mather, A. E. The Solubility of Carbon-Dioxide in Water at Low-Pressure. *J. Phys. Chem. Ref. Data* **1991**, *20*, 1201−1209.

(48) Liu, X. J.; Sun, L.; Deng, W. Q. Theoretical Investigation of CO2 Adsorption and Dissociation on Low Index Surfaces of Transition Metals. *J. Phys. Chem. C* **2018**, *122*, 8306−8314.

(49) Jin, W.; Wang, Y.; Liu, T.; Ding, C.; Guo, H. CO2 chemisorption and dissociation on flat and stepped transition metal surfaces. *Appl. Surf. Sci.* **2022**, *599*, 154024.

(50) Tanaka, K.; White, J. M. Dissociative adsorption of carbon dioxide on oxidized and reduced platinum/titanium dioxide. *J. Phys. Chem.* **1982**, *86*, 3977−3980.

(51) Taylor, C. D.; Neurock, M. Theoretical insights into the structure and reactivity of the aqueous/metal interface. *Curr. Opin. Solid State Mater. Sci.* **2005**, *9*, 49−65.

(52) Yoon, Y.; Rousseau, R.; Weber, R. S.; Mei, D.; Lercher, J. A. First-Principles Study of Phenol Hydrogenation on Pt and Ni Catalysts in Aqueous Phase. *J. Am. Chem. Soc.* **2014**, *136*, 10287−10298.

(53) Jinnouchi, R.; Anderson, A. B. Electronic structure calculations of liquid-solid interfaces: Combination of density functional theory and modified Poisson-Boltzmann theory. *Phys. Rev. B: Condens. Matter Mater. Phys.* **2008**, *77*, 245417.

(54) Li, G.; Wang, B.; Resasco, D. E. Solvent effects on catalytic reactions and related phenomena at liquid-solid interfaces. *Surf. Sci. Rep.* **2021**, *76*, 100541.

(55) Agirrezabal-Telleria, I.; Iglesia, E. Mechanistic insights and consequences of intrapore liquids in ethene, propene, and butene dimerization on isolated Ni2+ sites grafted within aluminosilicate mesopores. *J. Catal.* **2020**, *389*, 690−705.

(56) Kadam, S. A.; Hwang, A.; Iglesia, E. Consequences of Intrapore Liquids on Reactivity, Selectivity, and Stability for Aldol Condensation Reactions on Anatase TiO2 Catalysts. *ChemCatChem* **2022**, *14*, No. e202200059.

(57) Urey, H. C.; Rittenberg, D. Some Thermodynamic Properties of the H1H2, H2H2Molecules and Compounds Containing the H2 Atom. *J. Chem. Phys.* **1933**, *1*, 137−143.

(58) Baird, T.; Paal, Z.; Thomson, S. J. Sintering studies on platinum black catalysts. Part 2.—Effect of temperature of treatment and method of preparation on the sintering process. *J. Chem. Soc., Faraday Trans. 1* **1973**, *69*, 1237−1241.

(59) Baird, T.; Paal, Z.; Thomson, S. J. Sintering studies on platinum black catalysts. Part 1.—Effect of pretreatment and reaction on particle size. *J. Chem. Soc., Faraday Trans. 1* **1973**, *69*, 50−55.

(60) Hassan, S. A. Kinetics of Sintering of Unsupported Platinum Catalyst in Nitrogen, Oxygen and Hydrogen Atmospheres. *J. Appl. Chem. Biotechnol.* **1974**, *24*, 497−503.

(61) Barrett, E. P.; Joyner, L. G.; Halenda, P. P. The Determination of Pore Volume and Area Distributions in Porous Substances. I. Computations from Nitrogen Isotherms. *J. Am. Chem. Soc.* **1951**, *73*, 373−380.

(62) Wolf, D.; Barre-Chassonnery, M.; Hohenberger, M.; van Veen, A.; Baerns, M. Kinetic study of the water-gas shift reaction and its role in the conversion of methane to syngas over a Pt/MgO catalyst. *Catal. Today* **1998**, *40*, 147−156.

(63) Phatak, A. A.; Delgass, W. N.; Ribeiro, F. H.; Schneider, W. F. Density Functional Theory Comparison of Water Dissociation Steps on Cu, Au, Ni, Pd, and Pt. *J. Phys. Chem. C* **2009**, *113*, 7269−7276.

(64) Tsai, C.; Lee, K.; Yoo, J. S.; Liu, X.; Aljama, H.; Chen, L. D.; Dickens, C. F.; Geisler, T. S.; Guido, C. J.; Joseph, T. M.; et al. Direct Water Decomposition on Transition Metal Surfaces: Structural Dependence and Catalytic Screening. *Catal. Lett.* **2016**, *146*, 718−724.

(65) den Dunnen, A.; van der Niet, M. J. T. C.; Koper, M. T. M.; Juurlink, L. B. F. Interaction between H2O and Preadsorbed D on the Stepped Pt(553) Surface. *J. Phys. Chem. C* **2012**, *116*, 18706−18712.

(66) van der Niet, M. J. T. C.; den Dunnen, A.; Juurlink, L. B. F.; Koper, M. T. M. A detailed TPD study of H2O and pre-adsorbed O on the stepped Pt(553) surface. *Phys. Chem. Chem. Phys.* **2011**, *13*, 1629−1638.

(67) Lew, W.; Crowe, M. C.; Karp, E.; Lytken, O.; Farmer, J. A.; Arnadottir, L.; Schoenbaum, C.; Campbell, C. T. The Energy of Adsorbed Hydroxyl on Pt(111) by Microcalorimetry. *J. Phys. Chem. C* **2011**, *115*, 11586−11594.

(68) Lew, W. D.; Crowe, M. C.; Karp, E.; Campbell, C. T. Energy of Molecularly Adsorbed Water on Clean Pt(111) and Pt(111) with Coadsorbed Oxygen by Calorimetry. *J. Phys. Chem. C* **2011**, *115*, 9164−9170.

(69) Miller, J. T.; Meyers, B. L.; Modica, F. S.; Lane, G. S.; Vaarkamp, M.; Koningsberger, D. C. Hydrogen Temperature-Programmed Desorption (H2 TPD) of Supported Platinum Catalysts. *J. Catal.* **1993**, *143*, 395−408.

(70) Anderson, J. R. Particle size effects in metal catalysts. *Sci. Prog.* **1985**, *69*, 461−484.

(71) Karelovic, A.; Ruiz, P. CO2 hydrogenation at low temperature over Rh/γ-Al2O3 catalysts: Effect of the metal particle size on catalytic performances and reaction mechanism. *Appl. Catal., B* **2012**, *113−114*, 237−249.

(72) Stará, I.; Nehasil, V.; Matolín, V. The influence of particle size on CO oxidation on Pd/alumina model catalyst. *Surf. Sci.* **1995**, *331−333*, 173−177.

(73) Fajin, J. L. C.; D S Cordeiro, M. N.; Gomes, J. R. B. Density Functional Theory Study of the Water Dissociation on Platinum Surfaces: General Trends. *J. Phys. Chem. A* **2014**, *118*, 5832−5840.

(74) Elliott, J. R.; Lira, C. T. *Introductory Chemical Engineering Thermodynamics*, 2nd ed.; Prentice Hall: Upper Saddle River, NJ, 2012; p xxvii, 876 p.

(75) Poling, B. E.; Prausnitz, J. M.; O'Connell, J. P. *The Properties of Gases and Liquids*, 5th ed.; McGraw-Hill: New York, 2001; p 768.

(76) Emmett, P. H.; Brunauer, S. The use of low temperature van der Waals adsorption isotherms in determining the surface area of iron synthetic ammonia catalysts. *J. Am. Chem. Soc.* **1937**, *59*, 1553−1564.

(77) Al-Abadleh, H. A.; Grassian, V. H. FT-IR Study of Water Adsorption on Aluminum Oxide Surfaces. *Langmuir* **2003**, *19*, 341−347.

(78) Agirrezabal-Telleria, I.; Iglesia, E. Stabilization of active, selective, and regenerable Ni-based dimerization catalysts by condensation of ethene withinordered mesopores. *J. Catal.* **2017**, *352*, 505−514.

(79) Zare, M.; Saleheen, M.; Kundu, S. K.; Heyden, A. Dependency of solvation effects on metal identity in surface reactions. *Commun. Chem.* **2020**, *3*, 187.

(80) Kristoffersen, H. H.; Vegge, T.; Hansen, H. A. OH formation and H-2 adsorption at the liquid water-Pt(111) interface. *Chem. Sci.* **2018**, *9*, 6912−6921.

(81) Bregante, D. T.; Flaherty, D. W. Impact of Specific Interactions Among Reactive Surface Intermediates and Confined Water on Epoxidation Catalysis and Adsorption in Lewis Acid Zeolites. *ACS Catal.* **2019**, *9*, 10951−10962.

(82) Gonzo, E. E.; Boudart, M. Catalytic hydrogenation of cyclohexene: 3. Gas-phase and liquid-phase reaction on supported palladium. *J. Catal.* **1978**, *52*, 462−471.

(83) Madon, R. J.; Iglesia, E. Catalytic reaction rates in thermodynamically non-ideal systems. *J. Mol. Catal. A: Chem.* **2000**, *163*, 189−204.

https://doi.org/10.1021/acs.jpcc.3c04678
J. Phys. Chem. C 2023, 127, 22032−22048

(84) Alvarez, J.; Crovetto, R.; Fernández-Prini, R. The Dissolution of N2 and of H2 in Water from Room Temperature to 640 K. *Ber. Bunsen Ges. Phys. Chem.* **1988**, *92*, 935−940.

(85) Clay, C.; Haq, S.; Hodgson, A. Hydrogen bonding in mixed OH+H2O overlayers on Pt(111). *Phys. Rev. Lett.* **2004**, *92*, 046102.

(86) Bregante, D. T.; Chan, M. C.; Tan, J. Z.; Ayla, E. Z.; Nicholas, C. P.; Shukla, D.; Flaherty, D. W. The shape of water in zeolites and its impact on epoxidation catalysis. *Nat. Catal.* **2021**, *4*, 797−808.

(87) Lin, L.; Ge, Y.; Zhang, H.; Wang, M.; Xiao, D.; Ma, D. Heterogeneous Catalysis in Water. *JACS Au* **2021**, *1*, 1834−1848.

(88) Li, G.; Wang, B.; Resasco, D. E. Water-Mediated Heterogeneously Catalyzed Reactions. *ACS Catal.* **2020**, *10*, 1294−1309.

(89) Abel, B.; Buck, U.; Sobolewski, A. L.; Domcke, W. On the nature and signatures of the solvated electron in water. *Phys. Chem. Chem. Phys.* **2012**, *14*, 22−34.

(90) Gaiduk, A. P.; Pham, T. A.; Govoni, M.; Paesani, F.; Galli, G. Electron affinity of liquid water. *Nat. Commun.* **2018**, *9*, 247.

(91) Musumeci, F.; Pollack, G. H. Influence of water on the work function of certain metals. *Chem. Phys. Lett.* **2012**, *536*, 65−67.

https://doi.org/10.1021/acs.jpcc.3c04678